Course G-7

CPHS Compact Pulsed Hadron Source

Introduction to Hadron Synchrotrons

Jie WEI（韦杰）

Tsinghua University, Beijing

清华大学 工程物理系 强子应用及技术中心

6th OCPA Accelerator School, Beijing, 2010-7-29 to 2010-8-7

Class Outline (I)

1. Overview
    - 1.1 History, trends, RCS vs. AR
    - 1.2 Low-loss design philosophy
2. Accelerator system: design & technical issues
    - 2.1 Lattice
    - 2.2 Acceptance, emittance, beam scraping & collimation
    - 2.3 Injection
    - 2.4 Acceleration
    - 2.5 Extraction
    - 2.6 Magnet system & field error compensation
    - 2.7 Vacuum chamber & shielding
    - 2.8 Beam diagnostics & machine protection

Class Outline (II)

3. Beam dynamics: intensity limiting mechanisms
   - 3.1 Transverse tune shifts & resonances
   - 3.2 Beam loss mechanisms
   - 3.3 Collective effects
   - 3.4 Electron cloud effects
   - 3.5 Computer simulation codes
4. Future applications & developments

References

Problems

1. Overview

1.1 History, trends,
rapid cycling synchrotron vs.
accumulator ring

History (what made it possible?)

- 1945 (E.M. McMillan, V.Veksler):
  Synchrotron
- 1950 – 1952 (E.D. Courant, M.S. Livingston, H.S. Snyder, N.C. Christofilos):
  Alternating-Gradient focusing
- Development of intense H^- and H^+ source
- 1970 (I.M. Kapchinskii, V.A. Teplyakov):
  Radio Frequency Quadrupole
- Linac development:
  - Permanent magnet quad for DTL, super-conducting RF, etc.

Intensity evolution of BNL AGS

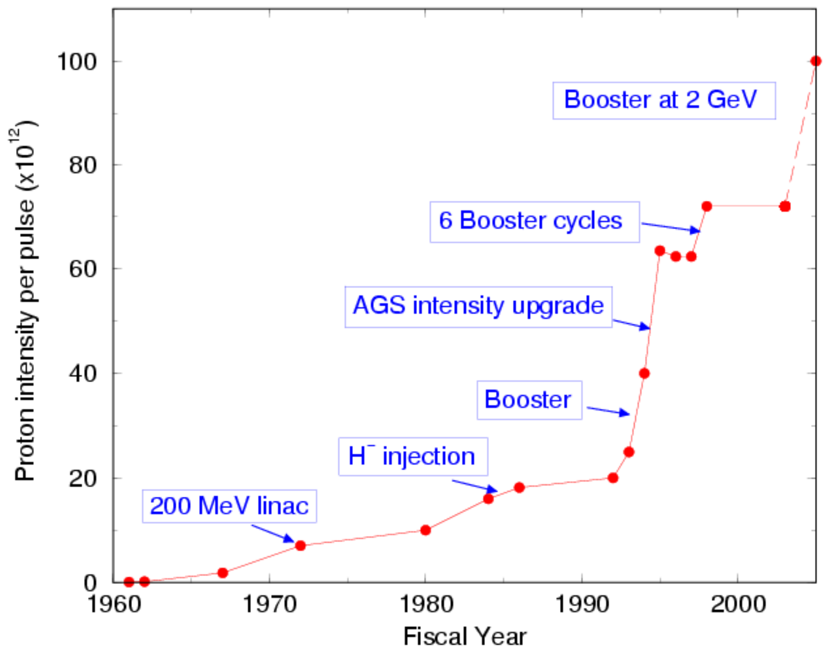

Accelerators at the power frontier

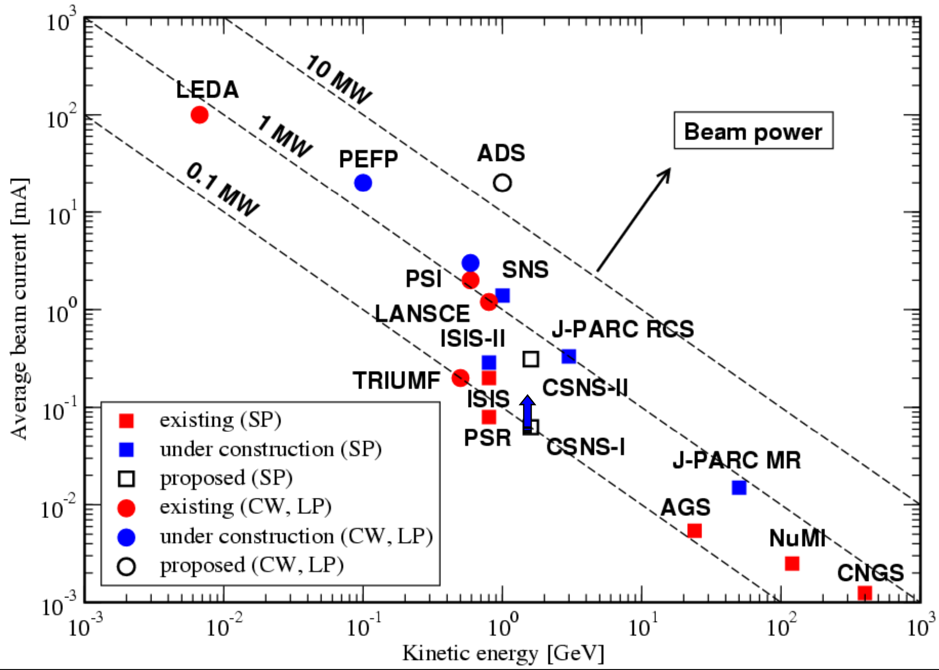

Evolution of ring beam intensity

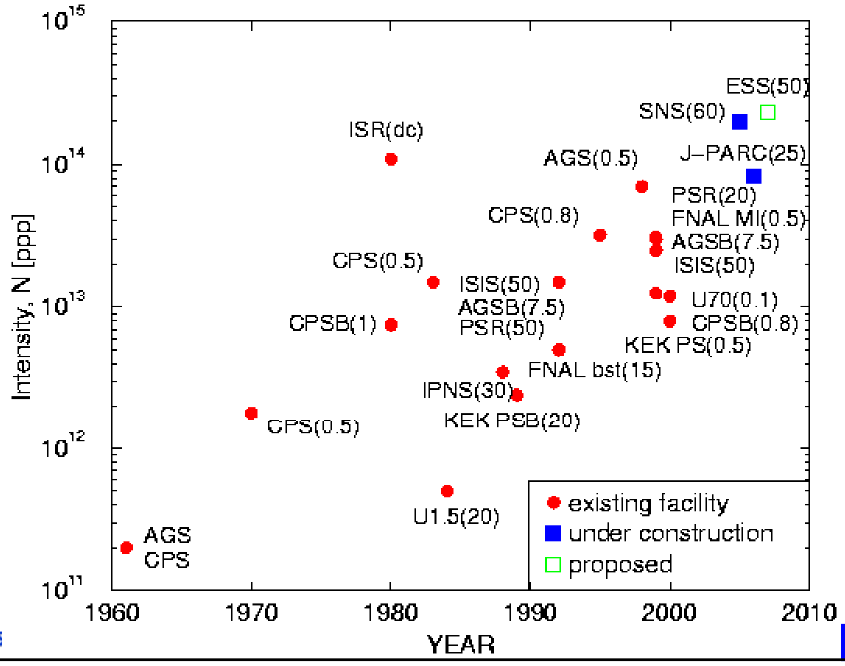

Mega-Watt project examples

	Energy [GeV]	Current [mA]	Rep.-rate [Hz]	Ave. power [MW]	Type
SNS	1	1.5	60	1.4	AR
J-PARC	3	0.33	25	1	RCS
CERN PD	2	2	100	4	AR
RAL PD	5	0.4	25	2	RCS
FNAL PD	16	0.25	15	2	RCS
EA	1	10 -- 20	CW	10 -- 20	cyclotron
APT	1.03	100	CW	103	linac
TRISPAL	0.6	40	CW	24	linac
ADTW	0.6 – 1.2	20 -- 50	CW	> 20	linac
μ-collider driver	30	0.25	15	7.0	RCS

J-PARC schematic layout

Japan Proton Accelerator Research Complex

Similar cost, similar schedule (due 2006 ~ 2007)

Ring clusters with expandable energy range; multipurpose

(Courtesy J-PARC)

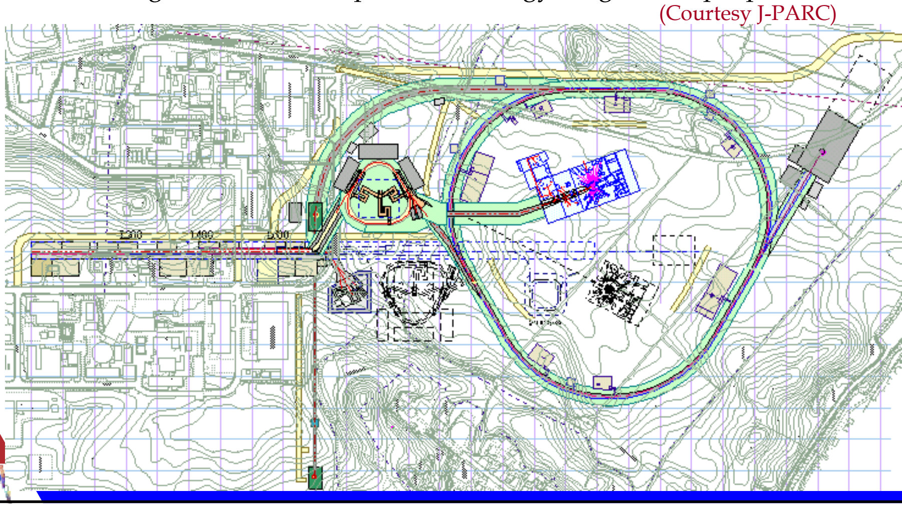

SNS schematic layout

- Built on top of the ridge, expandable with a 2nd target (but wrong location for a long pulse target station)
- Extra long linac tunnel is reserved for future energy/power upgrade; ring capacity reserved

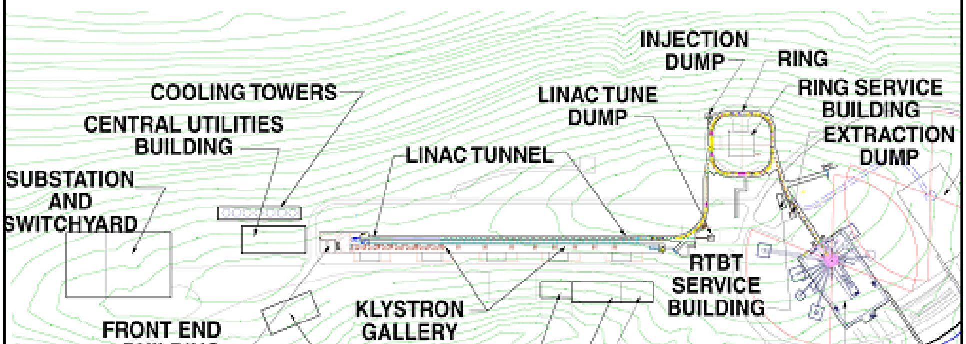

Pulsed accelerator options:

- Full energy linac & accumulator ring
  - Simpler ring design, no magnet ramping, better field quality
  - Shorter ring storage time, less instability, lower beam loss
  - Not compatible to energy/power upgrade
  - Longer, more expensive linac
- Low energy linac & rapid cycling synchrotron
  - Easy on energy/power upgrade with additional RCSs
  - Less overall cost for facilities of lower (<1 MW) beam power
  - More RF, higher magnet strength for ring
  - Difficult to control beam loss

SNS ring design debates

- Accumulator or rapid-cycling synchrotron?
  - Loss-power comparison: PSR loss 0.3%; usual RCS loss ~10%
  - RF, power supply, beam-pipe shielding, magnetic & track errors
- FODO-doublet lattice or all-FODO lattice?
  - Long, matched straight section: injection independent of tuning; collimation efficiency from ~ 80% to 95%
- Do we need sextupoles? Energy corrector & spreaders?
  - Four-family chromatic sextupole for tune-spread control & match
  - Energy correctors & spreaders for longitudinal painting
- Can we use permanent magnets? Certainly not for a cold linac!
- Should the aperture be reduced? No, aperture is everything!
- Solid-core or laminated-core magnets (*)?
  - Large field variation in a solid-core magnet (although lower cost)

1.2 Low-loss design philosophy

Low-loss design philosophy

- Localize beam loss to shielded area
  - 2-stage collimation, 3-step beam-gap chopping/cleaning
- A low-loss design
  - Proper lattice design with adequate aperture & acceptance $A/\varepsilon>2$
  - Injection painting; Injection & space-charge optimization $\Delta Q<0.2$
  - Resonance minimization; Magnet field compensation & correction
  - Impedance & instability control
- Flexibility
  - Adjustable energy, tunes; Flexible injection; Adjustable collimation
  - Foil & spare interchange
- Engineering reliability: heat & radiation resistant
- Accidental prevention: Immune to front end, linac & kicker fault

Secondary collector design

Length enough to stop primary protons (~ 1 m for 1 GeV beam)

Layered structure (stainless steel particle bed in borated water, stainless steel blocks) to shield the secondary (neutron, γ)

Fixed, enclosing elliptical-shaped wall for operational reliability

Double-wall Inconel filled with He gas for leak detection

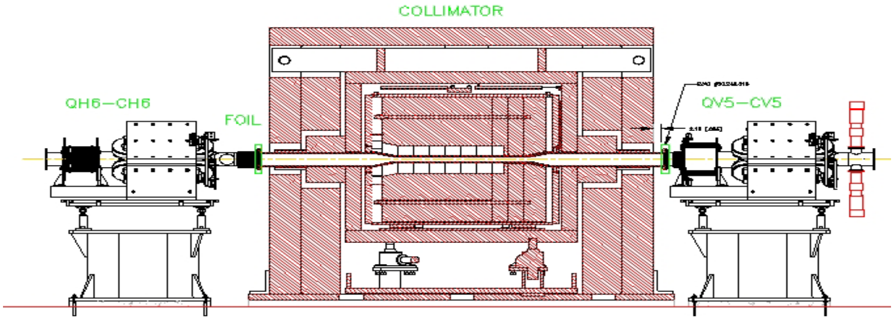

2. Accelerator system: design & technical issues

2.1 Lattice

Symmetry, resonance, free space

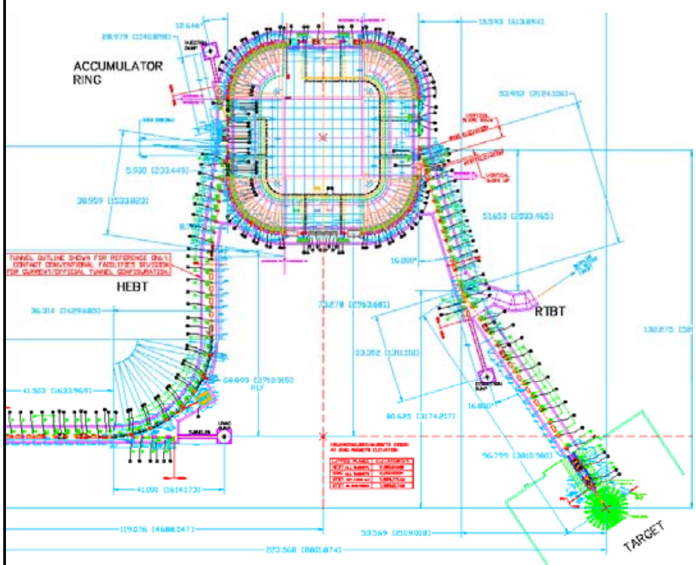

- higher symmetry, fewer structural resonances
- lower symmetry, longer free space

TABLE I. Examples of favorable working points in the transverse tune space for some existing and designed rings for high-intensity operations (Sec. III.A.5).

Machine	Superperiodicity	Horizontal tune	Vertical tune	Proton per pulse
Operating:				
AGS	12	8.8	8.9	7×10^{13}
AGS Booster	6	4.8	4.9	2.3×10^{13}
CERN's PSB	16	4.28	5.56	1.3×10^{13}
CERN's PS	10	6.25	6.30	3.2×10^{13}
CERN's SPS	6	26.62	26.58	4.6×10^{13}
FNAL's Booster	24	6.7	6.8	5×10^{12}
FNAL's MI	2	26.425	25.415	3×10^{13}
IPNS	6	2.20	2.32	3.5×10^{12}
ISIS	10	4.31	3.83	2.5×10^{13}
KEK's PSB	8	2.17–2.10	2.30–2.40	2.4×10^{12}
KEK's PS	4	7.14–7.16	5.24	8×10^{12}
PSR	10	3.19	2.19	5×10^{13}
U1.5	12	3.92	3.75	5×10^{11}
U70	12	9.92	9.85	1.2×10^{13}
Designed:				
ESS	3	4.19	4.31	2.3×10^{14}
J-PARC 3-GeV	3	6.72	6.35	8.3×10^{13}
J-PARC 50-GeV	3	22.4	22.25	3.3×10^{14}
SNS	4	6.23	6.20	2×10^{14}

SNS ring schematic

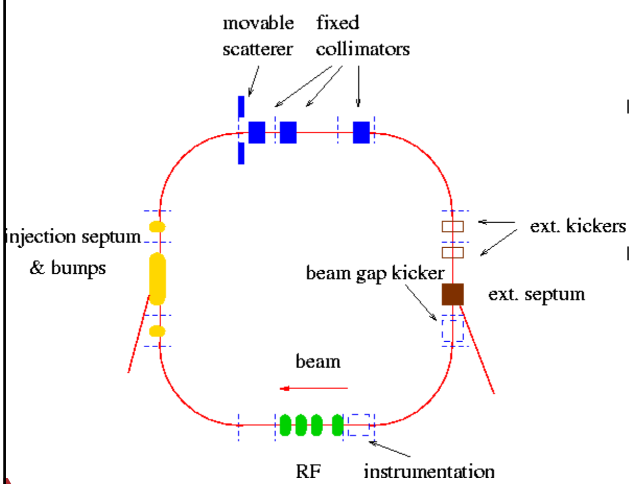

- FODO
  - Modest quad strength
  - Easy for correction (alternating β functions)
- Doublet:
  - Long uninterrupted straights
  - Less joints, bellows, vacuum chambers
- Four straights with separate functions
  - Injection modules
  - Two-stage collimation
  - Extraction & Beam-in-gap kickers
  - 3(h=1)&1(h=2) RF cavities

CPHS

22

Ring arc

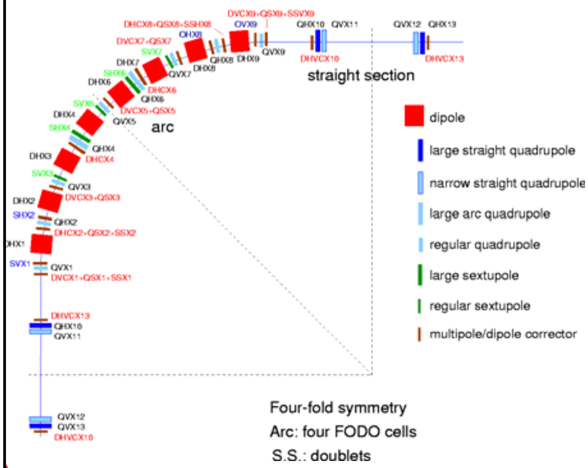

- FODO/Doublet (hybrid) lattice
- 32 dipoles, 52 quadrupoles
- Chromatic correction with 20 arc sextupoles
- Orbit/coupling correction with correctors in the arcs
- Resonance correction in arc and straights

CPHS

Optics functions and matching

- First find the strengths of the two arc quadrupole families to get an horizontal phase advance of 2π and using the vertical phase advance as a parameter
- Then match the straight section with arc by using the two doublet quadrupole families and the matching quad at the end of the arc in order to get the correct tune without exceeding the maximum beta function constraints
- Retune arc quads to get correct tunes
- Always keep beta, dispersion within acceptance range and quadrupole strength below design values

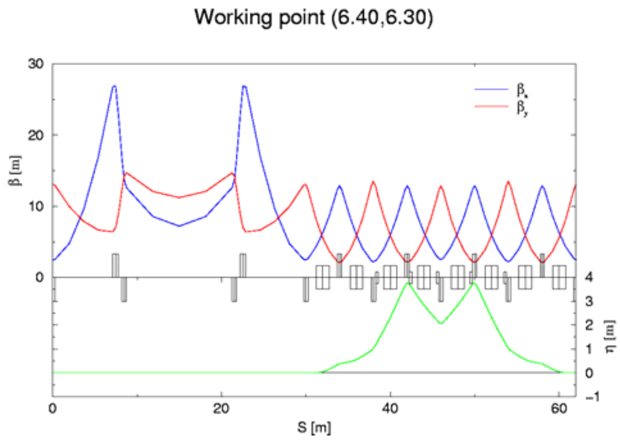

CPHS

CSNS RCS layout (2008)

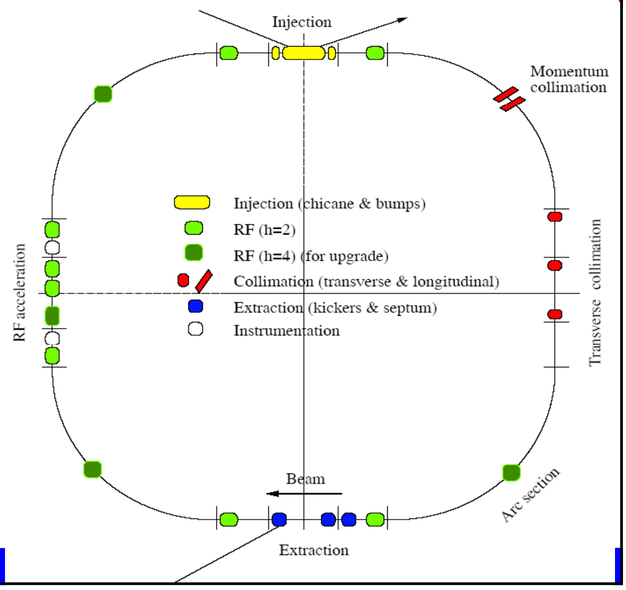

CSNS RCS lattice (2008)

- Four-fold symmetry
  - Separated functions
- FODO arc (3.5 cell at each arc)
  - Easy correction
- Dispersion-free doublet straight
  - long, uninterrupted straight for collimation & injection
- Missing-gap momentum collimation
  - High momentum cleaning efficiency
- Easy to modify
  - New lattice for longer straight sections

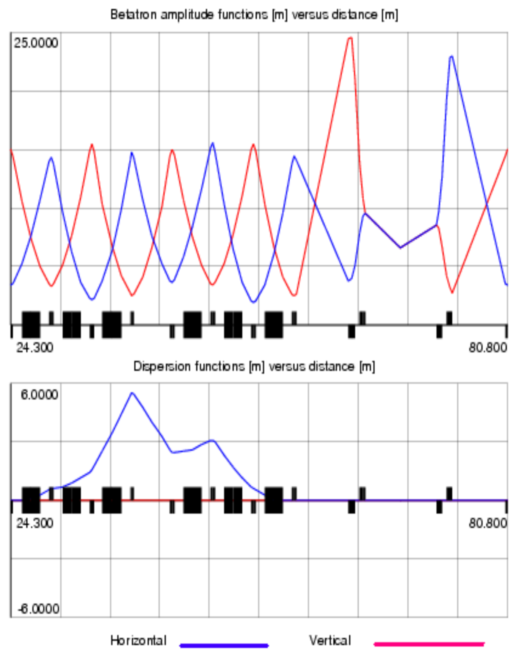

SNS ring tune space

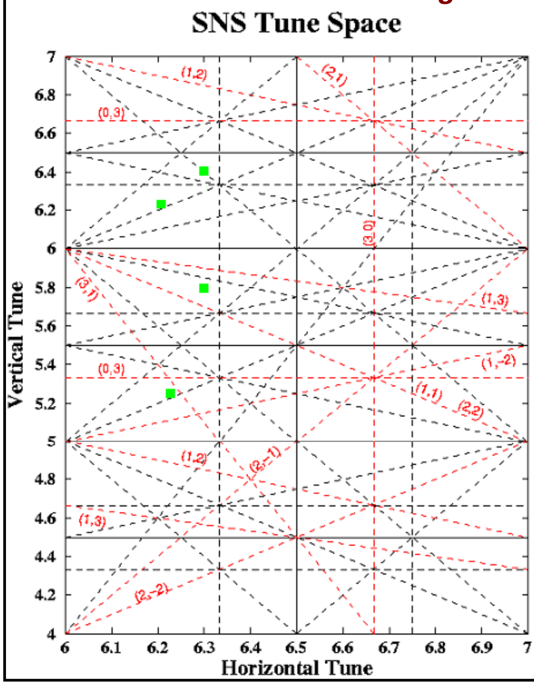

Tuneability: 1 unit in horizontal, 3 units in vertical (2 units due to bump/chicane perturbation)

– **Structural resonances (up to 4th order)**

– **All other resonances (up to 3rd order)**

- **Working points considered**
  - **(6.30,5.80) - Old**
  - **(6.23,5.24)**
  - **(6.23,6.20) - Nominal**
  - **(6.40,6.30) - Alternative**

ISIS tune variation along ramp

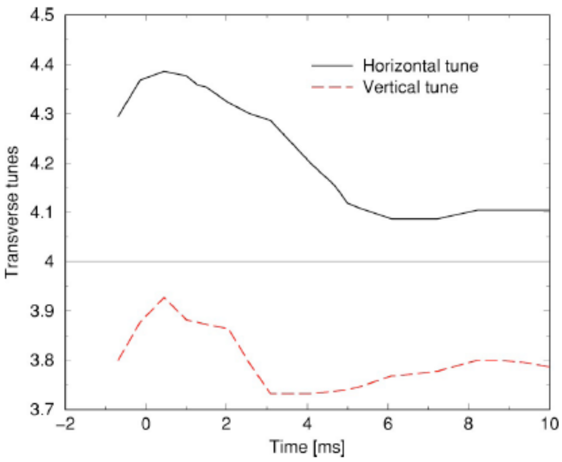

- compensate for the natural chromaticity and the varying magnet field at injection,
- ramp up tunes to minimize effects of space charge depressions during beam capture
- reduce tunes during the time from 2 to 4 ms after injection to avoid transverse resistive wall instability
- lower tunes to avoid coupling resonances at extraction.

2.2 Acceptance, emittance, beam scraping & collimation

Transverse acceptance

- Transverse motion

$$x(s) = x_\beta(s) + x_p(s) + x_{c,0}(s) + x_c(s)$$

- Betatron amplitude, off-momentum closed orbit, design closed orbit, closed-orbit deviation

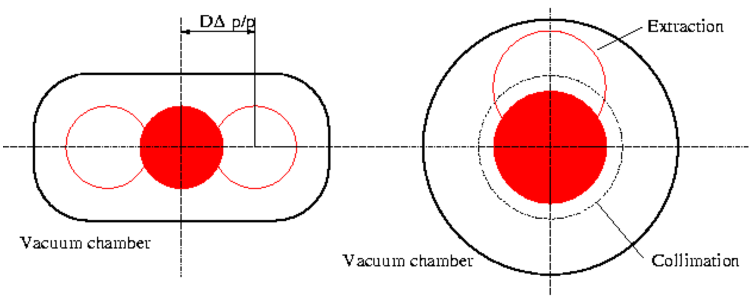

Arc

Straight

Typical dipole vacuum chamber

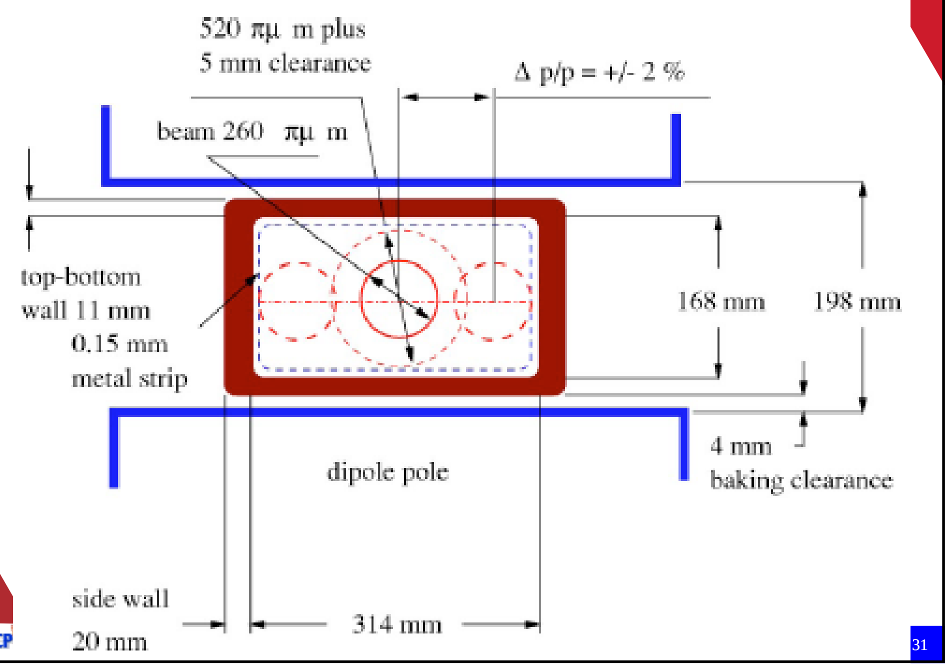

Injection straight section example

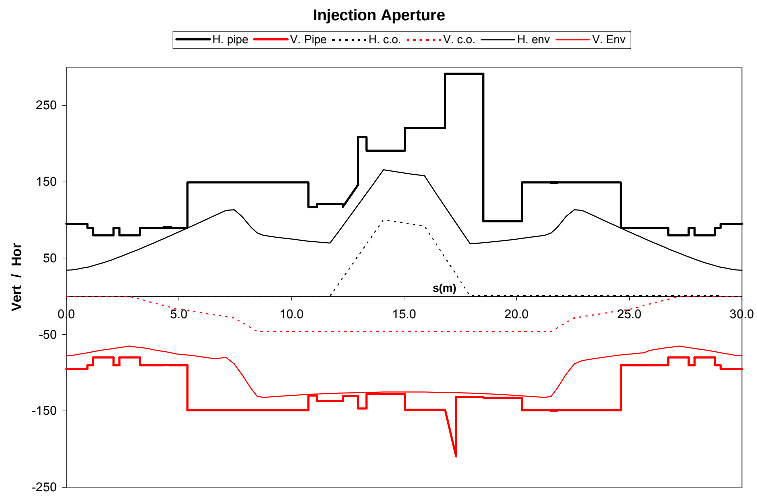

Longitudinal acceptance

- Momentum acceptance from transverse aperture at high-dispersion region
- RF bucket admittance
- Beam gap reserve

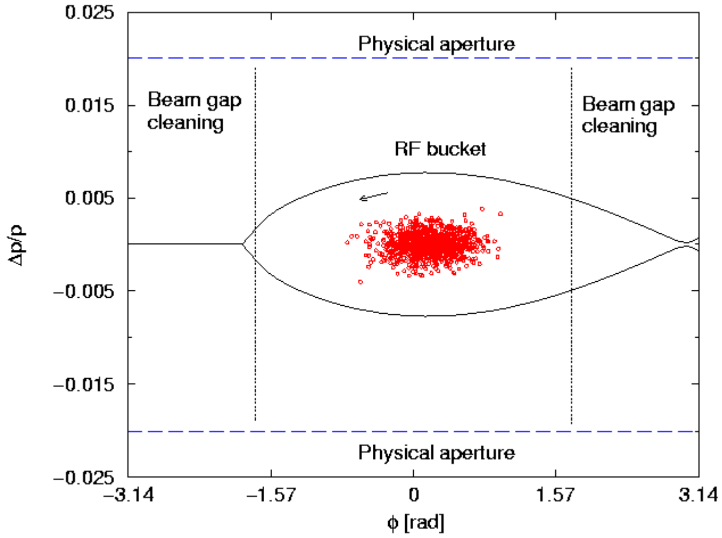

Collimation optimization

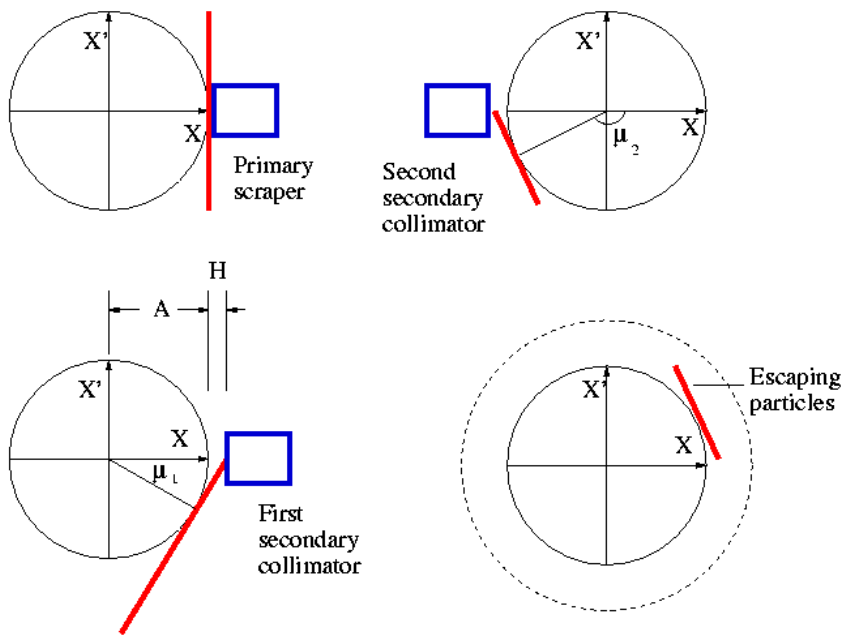

Collimator design

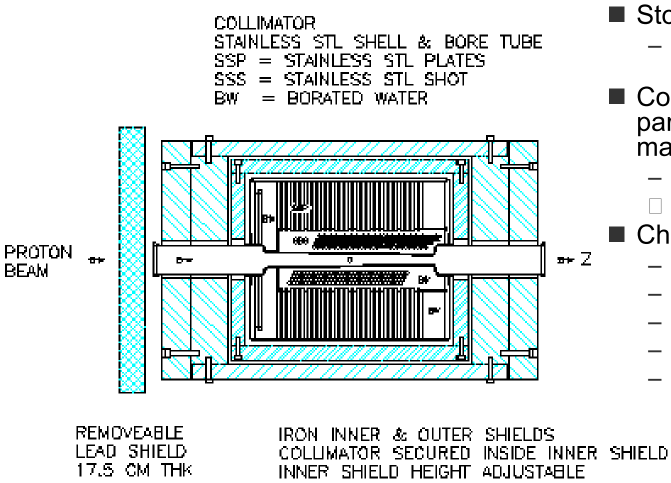

- Stops primary proton
  - Longer length for higher energy
- Contains secondary particles with layered material
  - Neutron
  - γ ray
- Choice of material
  - Vacuum out-gassing
  - Secondary scattering
  - Heat resistance
  - Radiation resistance
  - Stopping capability

courtesy H. Ludewig, N. Catalan-Lasheras

SCHEMATIC OF COLLIMATOR COMPONENTS
HORIZONTAL SECTION

35

Ring scraper & collimator

4 scrapers spaced at 45 degree angle

3 collimators; first one to shield scraper shine

Needs a large vacuum-pipe aperture and a long straight section

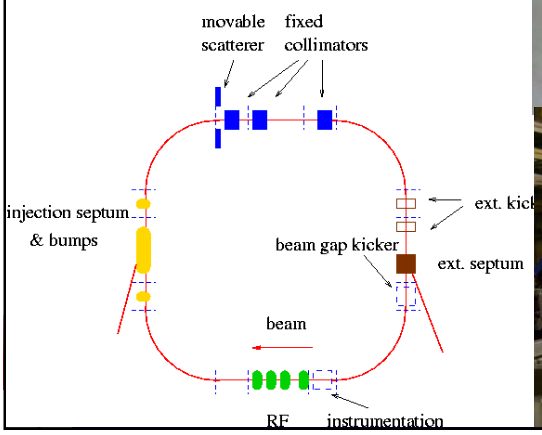

2.3 Injection

SNS ring injection layout

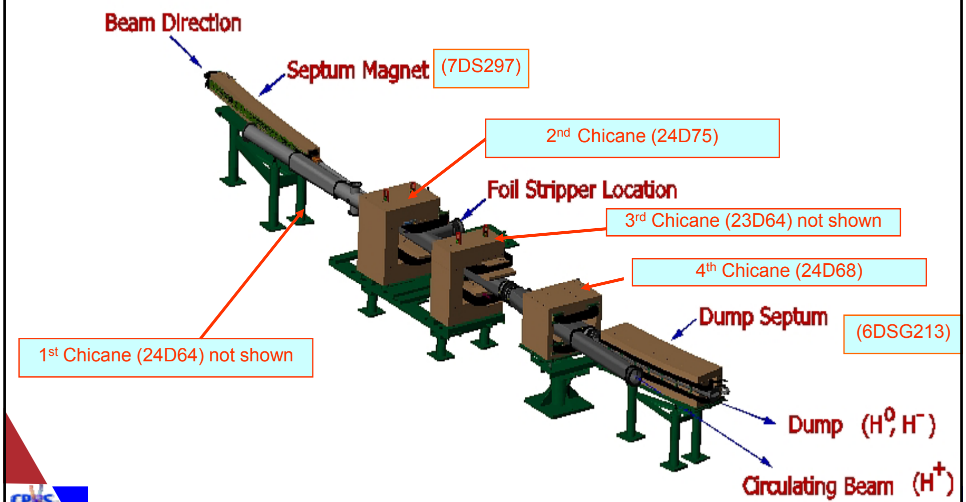

SNS injection layout

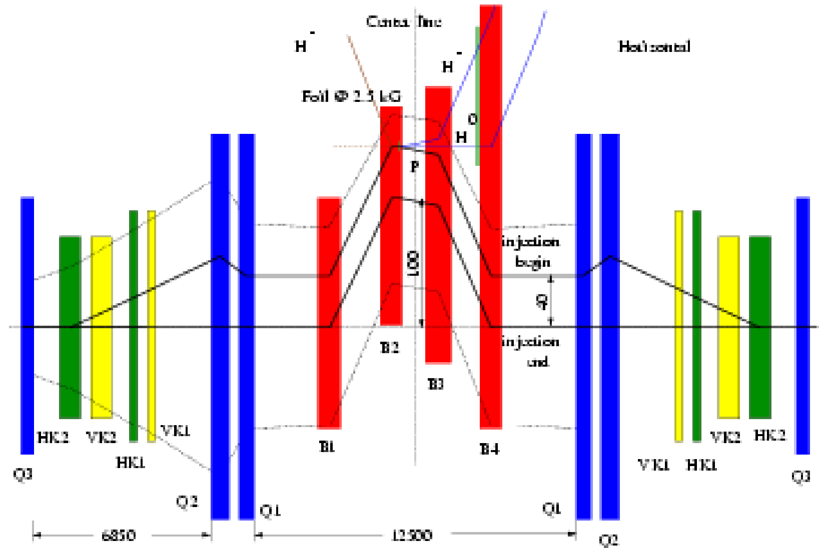

- Horizontal: 2 sets of 4-bumps super-imposed (red and green)
- Green magnets: horizontal 4-bump for painting
- Yellow magnets: vertical 4-bump for painting
- Red: fixed chicane dipoles

Correlated painting

- Parallel horizontal and vertical orbit bumps, from small to large amplitude

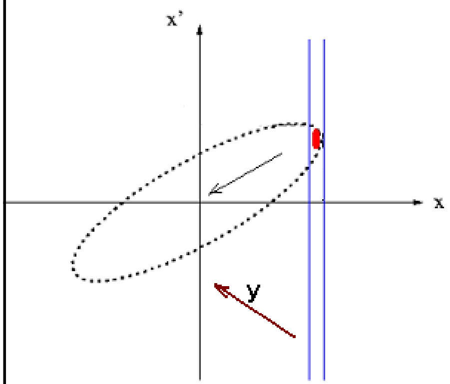

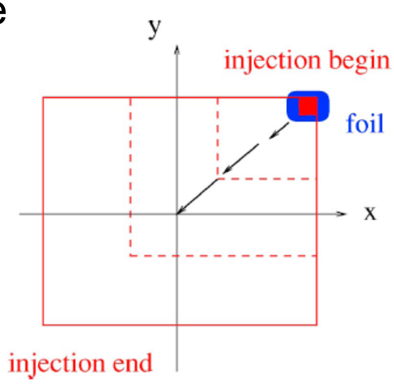

FIG. 26. (Color in online edition) Beam transverse profile of correlated bump painting used in charge-exchange injection into the SNS ring (Sec. III.C.4).

Vertical steering/horizontal painting

- Steer in one direction, painting in the other

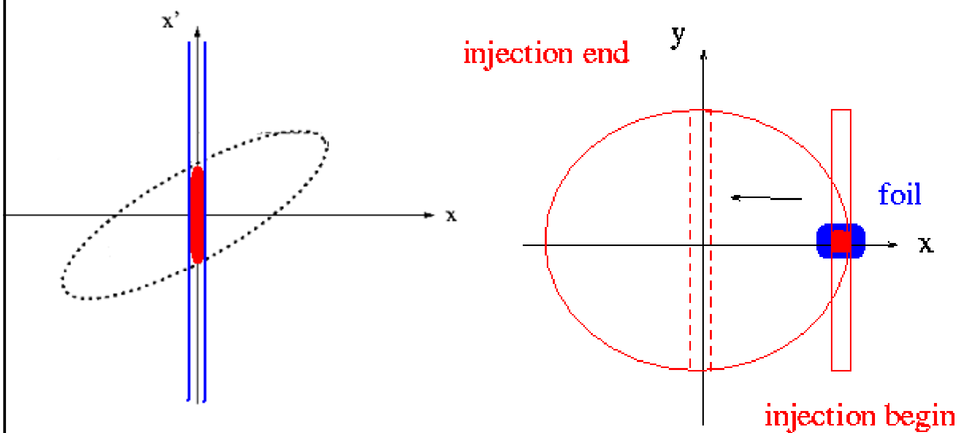

Space charge & halo formation

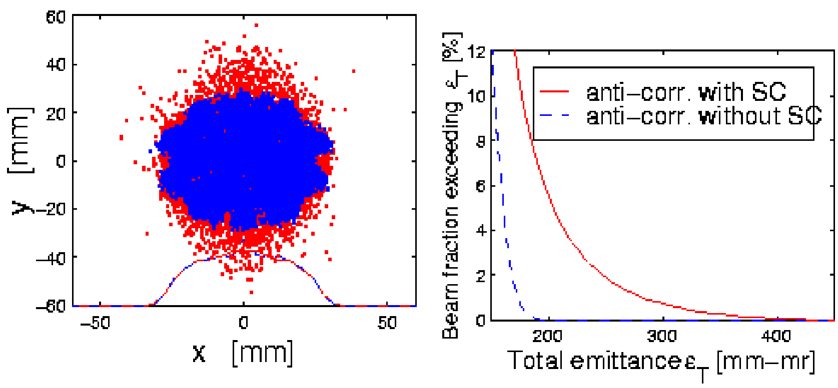

Disadvantage of not painting over halo (vertical direction)

Stripping of H^- and H^0

- General loss criteria for stripping in HEBT and injection:
  - < 10^{-7} per meter beam loss
- Gas stripping sets a limit on vacuum pressure
  - 5×10^{-8} ~ 10^{-7} Torr
- Electro-magnetic Lorentz stripping on H^- beam
  - Mean decay length in laboratory frame

$$\lambda_s = \frac{A_{s1}}{B} \exp \frac{A_{s2}}{\beta\gamma B},$$

$$A_{s1} = (2.47 \pm 0.09) \times 10^{-6} \text{ Tm, and } A_{s2} = 15.0 \pm 0.03 \text{ T}$$

  - Less that 3 kG field for 1 GeV beam
- H^0 stripping
  - Require specific field (<+/-5% error) maintain decay lifetime of certain quantum state (n=5) H^0 from pre-mature stripping
  - Foil residing in a trailing field at 2.4 kG

Collection of stripped electrons

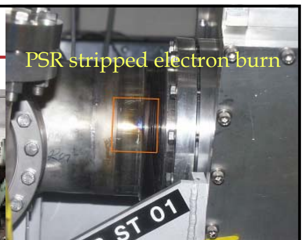

(Courtesy W. Meng, J. Brodowski, YY Lee, D. Abell, R. Macek et al)

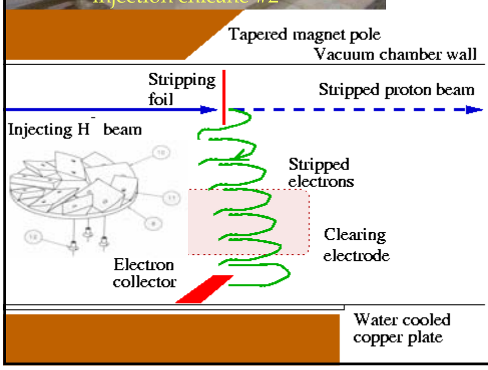

Tapered magnet to guide stripped electrons (~ 2 kW), compensated for the circulating beam
Carbon-carbon collector on water-cooled copper plate
Clearing electrode (~ 10 kV) to reduce scattered electrons
Video monitors on foil & collector

SNS injection foil device

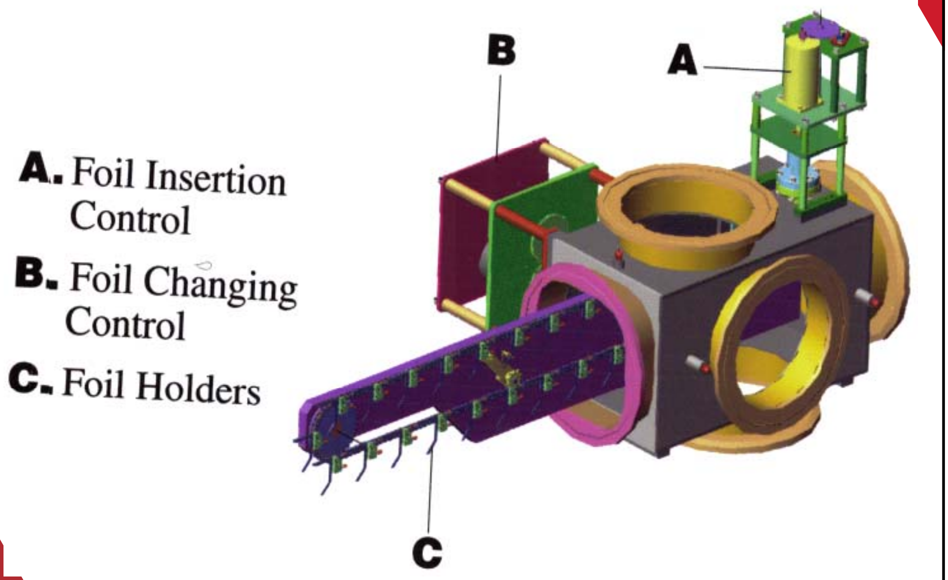

SNS injection kicker

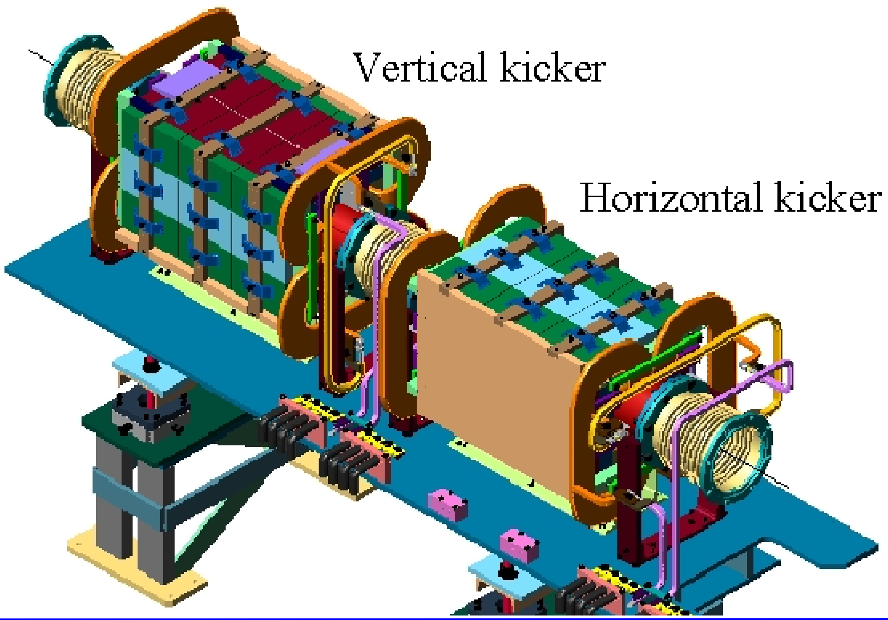

Injection vacuum chamber coating

(Hseuh, He, Todd …)
Injection kicker ceramic chamber double coating

Cu (~ 0.7 μm) for image current
TiN (0.1 μm) for electron cloud
Meets requirement: conductive coatings w/ end-to-end resistance of ~0.04Ω ± 50% (Henderson, Davino)
Thickness uniformity < ± 30%

Injection kicker time response measurement

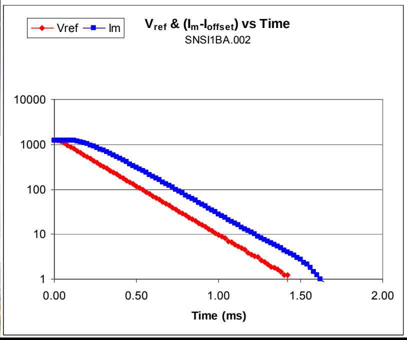

Expected time constant [ms]	0.15	0.2	0.25	0.3	0.4
Measured time constant [ms]	0.171	0.213	0.260	0.307	0.402

- Satisfactory time response (< 0.2 ms)
- Interference from vacuum chamber/coating not noticeable
  - 700 nm Cu and 100 nm TiN
- Need to verify magnet-to-magnet matching

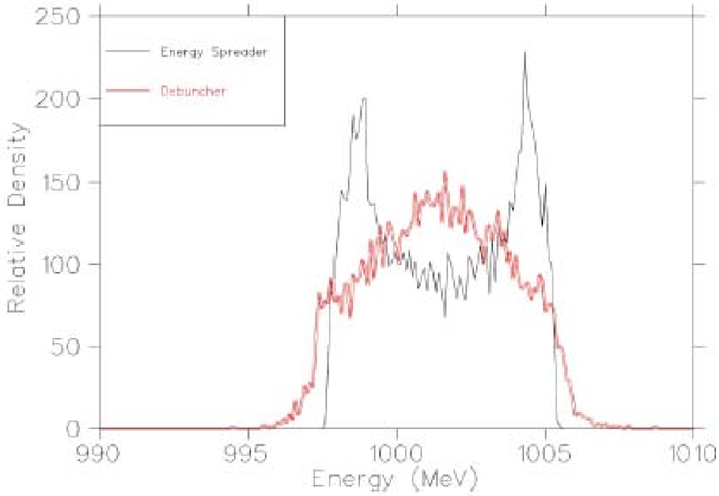

FIG. 28. (Color in online edition) Energy distribution at the injection foil, using either an energy spreader or a conventional debuncher. An energy spreader significantly suppresses the beam tail (Sec. III.C.4).

- "sharpen" the painting pen by reducing momentum spread before injection (correcting energy jitter, e.g.)
- Paint the momentum space by modulating the injecting beam energy

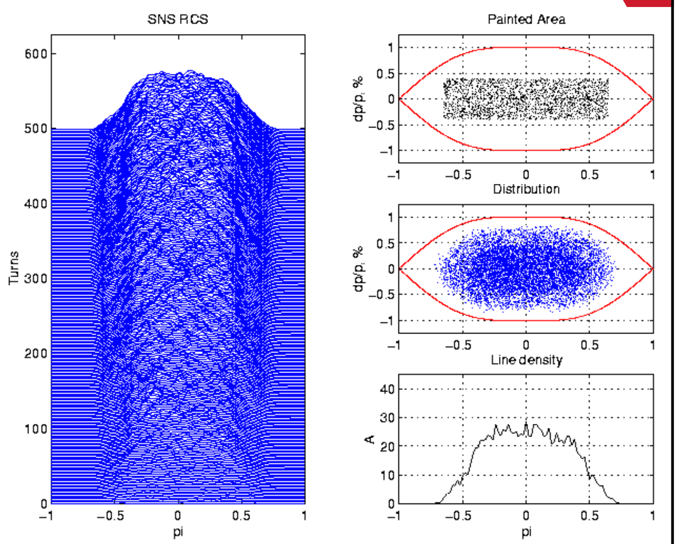

Figure 7: Longitudinal bunch evolution during injection with a dual ($h = 2$ and $h = 4$) RF system. The full injection momentum spread at the end of HEBT line is $\Delta p/p = \pm 0.4\%$, the peak current is 26 A, and the bunching factor is 0.46.

2.4 Acceleration

Ramping

- Prefers injection “flat-bottom” and extraction “flat-top”
- Simplest scheme for RCS: sinusoidal resonance ramp
- Possibly slower up-ramp and faster down-ramp
- Smooth variation of longitudinal parameters

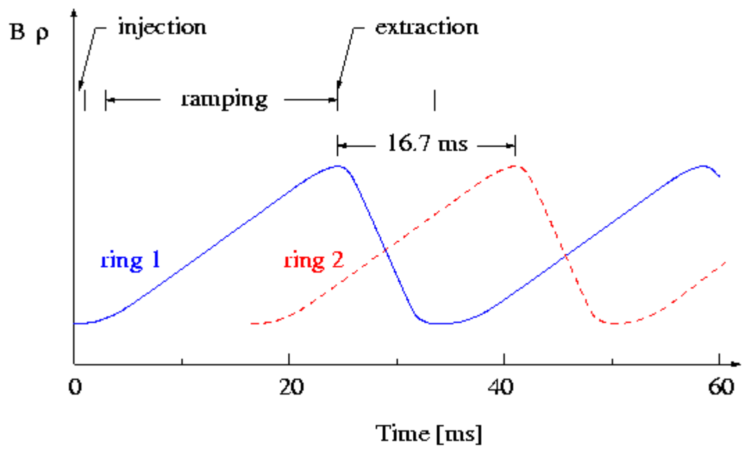

Program of RF voltage & phase

- Beam loss often occurs at initial ramping due to reduction in bucke area when the synchronous phas is increased
- Careful program o voltage and phase to ensure monotonic increas of bucket area
- Keep the process adiabatic

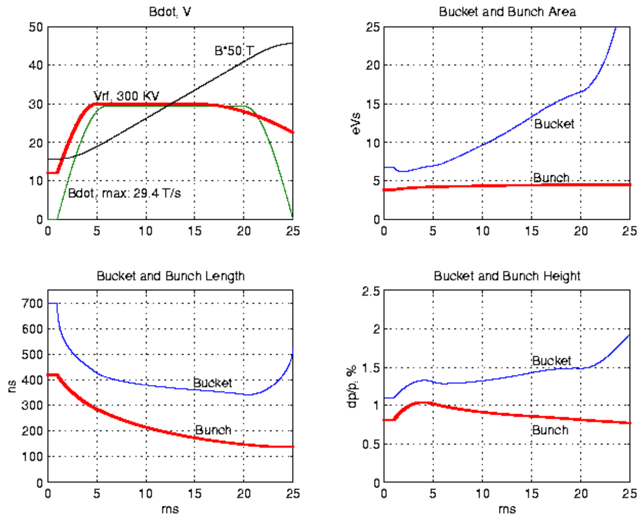

Figure 8: Programming of RF voltage and magnetic field, and the evolution of momentum spread, bunch area and bunch width in comparison with the $(h = 2)$ RF bucket.

SNS ring RF cavities

SNS RF system at ORNL

RF system components

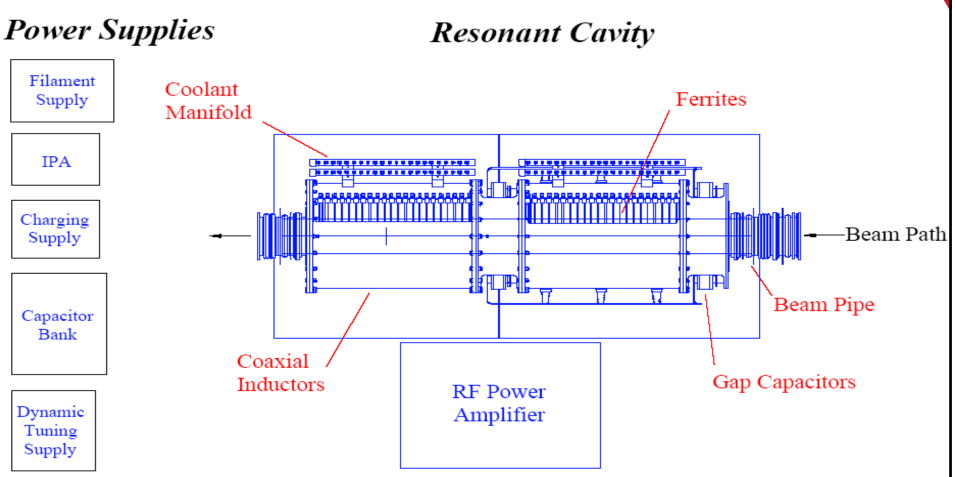

Ferrite-loaded cavities

- Frequently used when variable resonance frequency is needed to follow the change of beam speed
- Cavity acts as a resonance transformer with the beam as the secondary winding
- Ferrite serves two purposes
  - Enhances the magnetic field for given current, allowing a small cavity size
  - Allow dynamic tuning of the cavity

RF cavity gradient upgrade at J-PARC

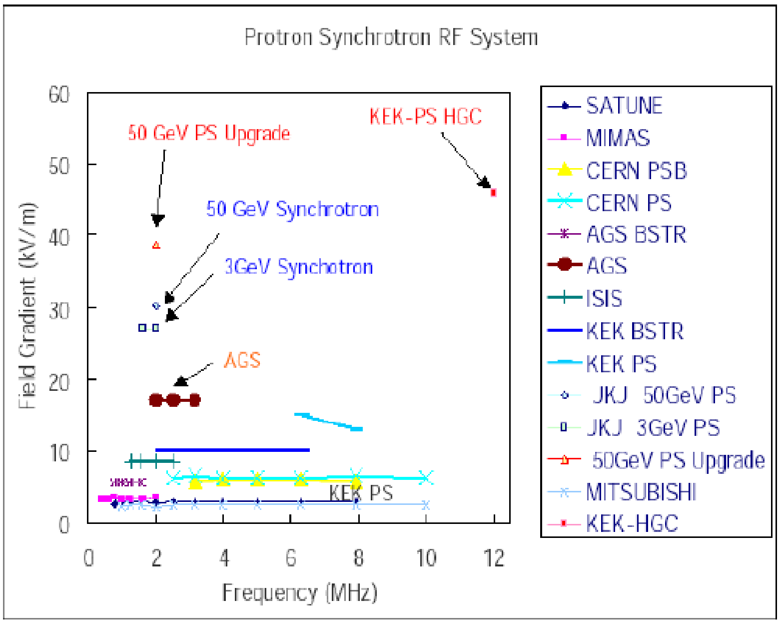

2.5 Extraction

Extraction (single-turn)

- Typical high-activation area
- Measures to control beam loss
  - Clean beam gap before extraction
  - Wide extraction channel, tolerable to 1 kicker failure
  - Beam position on target immune to kicker failure
- Impedance control
  - Kickers often reside inside vacuum chamber – needs to minimize coupling impedance and to perform special coating
- Maintainability
  - Remove device (pulse forming network, etc.) outside of tunnel

SNS extraction kicker (14 units)

- Ferrite kicker inside vacuum pipe to allow fast field variation
- Variable gap height/width (optimize impedance, power load, clearance)

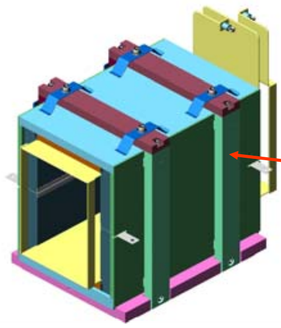

Magnet Type :WF (Ferrite)
Ferrite Length : 0.35 m
∫Bd*l* : 9.5 to 6.5 kGauss.cm
Gap (Hor.) : 13.8 to 19 cm
Width(Vert.): 13.1 to 24.8 cm
Rise time to 95% : 200 nsec
Maintain peak field: 750 nsec

Single kicker 3-D Calc.
∫Bd*l*=7.0 kGauss.cm/kicker
L=0.81 μH/kicker

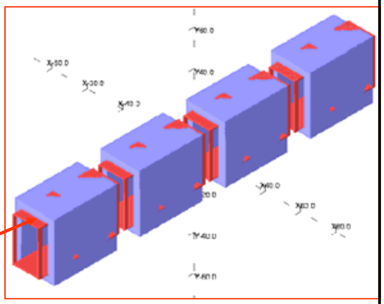

4-Kickers in Tandem
∫Bd*l*=6.75 kGauss.cm/kicker
L=0.87 μH/kicker

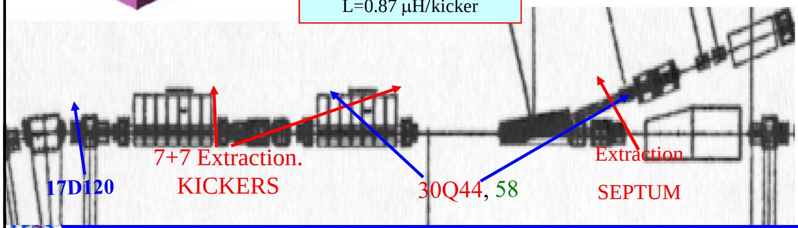

Extraction septum magnet

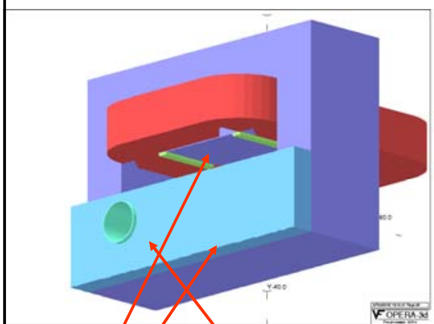

- Lambertson septum: avoids electrical elements between the circulating and extraction beam channels

Bend Angle : 16.8^0
Field Un. : $\Delta(\int Bdl)/(B_0L_{eff}) \leq \pm 1\times10^{-3}$
Iron Length : 2.44 m
∫Bd*l* : 1.58 Tm for 1.0 GeV
Magnet Gap : ~16.5 cm
Septum thickness : 1 cm
Pipe ID Circ Beam : 17.5 cm
∫Bd*l* at Circ Beam : ≤500 Gauss.cm

“Shims” of the Lambertson Septum

“Field Clam” and “Magnetic-pipe” to reduce stray fields at the circulating beam region

The B_{mod} of the stray fields at the center of the pipe of the circulating beam with and without “Field Clam”

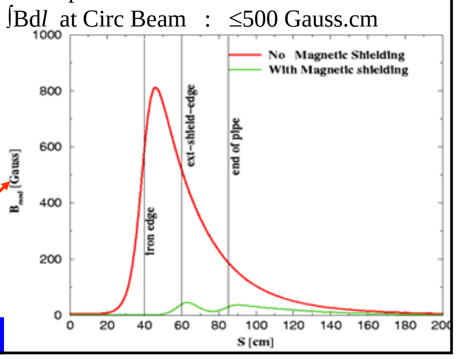

Kicker's pulse-forming network

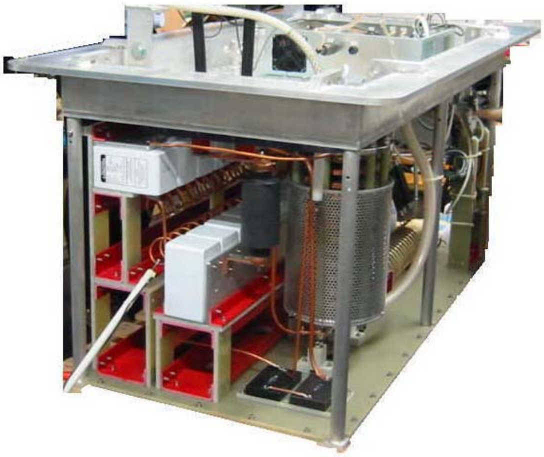

- Placed outside of the tunnel to avoid radiation damage
- Careful EMI isolation, ground break
- Optimize saturable inductor to effectively "shorten" rise time (200ns)
- Improved flat-top flatness (1%)
- PFN termination: lower impedance
- Increase magnet height to halve coupling impedance (same drive)
- Shield the terminating resistance, reducing cable reflection

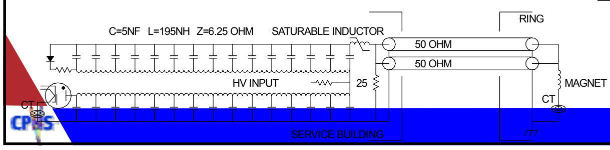

2.6 Magnet system & field error compensation

SNS AR: solid core dipole & quad magnets

J-PARC laminated magnets with stranded conductor & cuts

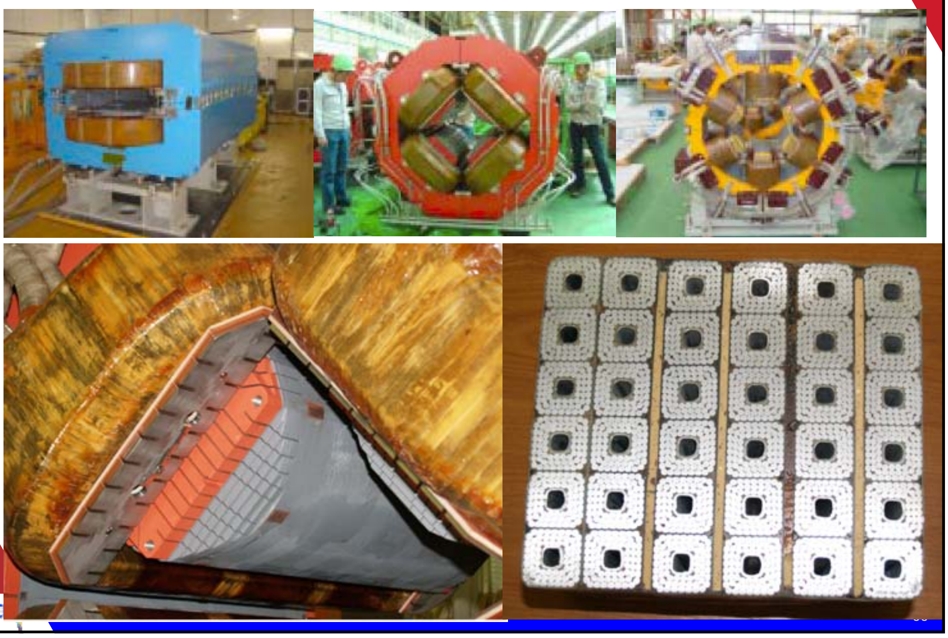

SNS figure-8 doublet quad & rad-hard quads

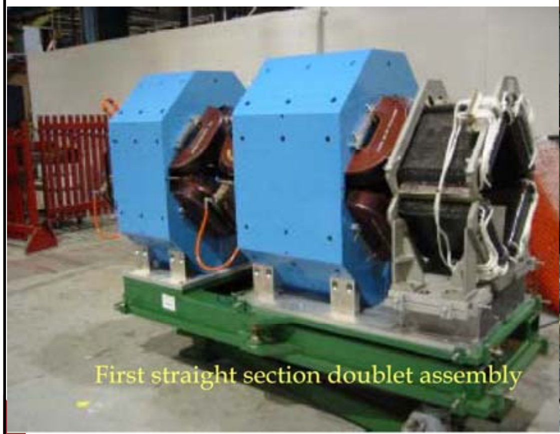

Magnet considerations

- High field
  - field saturation, high current engineering
- High repetition rate
  - Eddy current, special coil (e.g. stranded coil), magnet core cuts
- Large aperture
  - Large power supply
- Close to nearby magnets
  - High magnet fringe field effects

Typical dipole magnet

- Iron core
- Water-cooled windings
- Good field quality ($\sim 10^{-4}$) achievable with iron shaping

$$N_{coil} I = gH$$

g [m]: gap size, $N_{coil}/2$: number of turns on each pole, I [A]: current

$$B = \mu_0 N_{coil} I / g \quad \text{[T]}$$

$$\mu_0 = 4\pi 10^{-7}$$

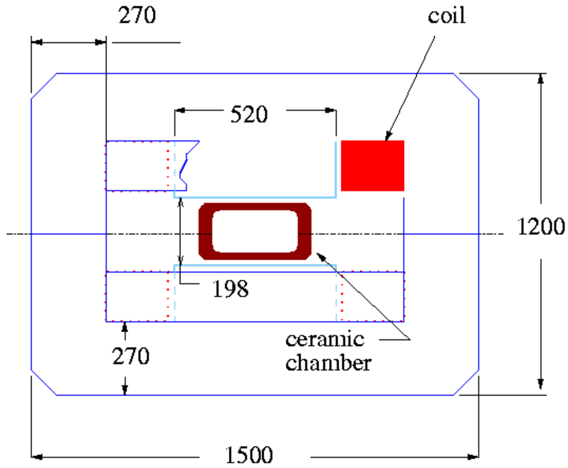

Magnet definitions

- 2m-pole:

dipole quadrupole sextupole octupole decapole …

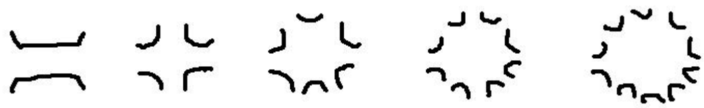

m: 1 2 3 4 5

- Normal: gap appears at the horizontal plane
- Skew: rotate around beam axis by $\pi/2m$ angle
- Symmetry: rotating around beam axis by π/m angle, the field is reversed (polarity flipped)

Magnetic multipole expression

- 2-D multipole expansion (European convention m->n+1)

$$B_y + iB_x = B_0 \sum_{n=0}^{\infty} (b_n + ia_n)(x+iy)^n$$

- Normalized units (reference radius, main field)

$$B_y + iB_x = 10^{-4} B_0 \sum_{n=0}^{\infty} (b'_n + ia'_n) \left(\frac{x+iy}{R_{ref}}\right)^n$$

$$2m(2k+1), \qquad k = 0,1,2...$$

- "Allowed multipoles": multipoles allowed by symmetry

Measured harmonics for SNS quadrupole 21Q40

n	a_n	b_n
1	-1.4 †	-58.1 †
2	0	$\boxed{10000}$
3	-0.1	1.6
4	-0.2	1.4
5	0.0	0.1
6	0.1	$\boxed{1.5}$
7	0.0	-0.1
8	-0.1	-0.2
9	0.0	0.1
10	0.0	$\boxed{-0.5}$
11	0.0	0.0
12	0.0	-0.1
13	0.0	0.0
14	0.0	$\boxed{-0.1}$

- The boxed values are the integrated harmonics allowed by quadrupole symmetry
- All harmonics are on the required within the required level of 10^{-4} of the quadrupole field
- Remark: the large values on the dipole terms are due to errors of the measuring coil location (0.5mm centering error)

SNS dipole integral transfer function

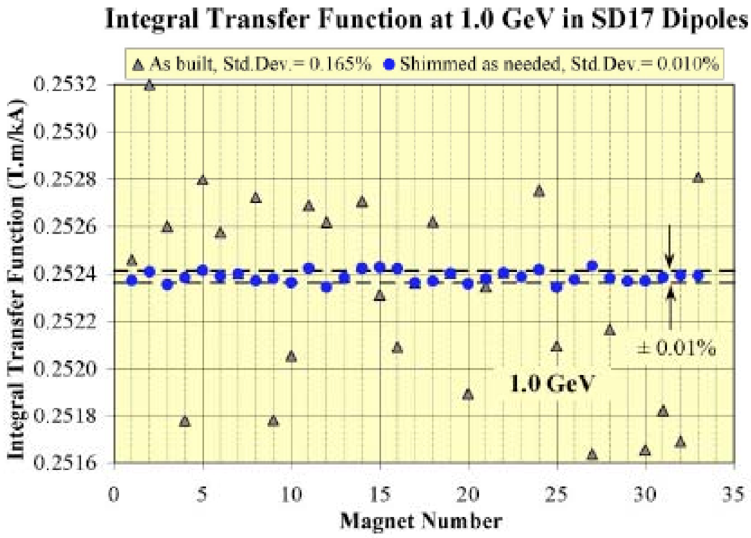

Shimming is optimized for 1.0 GeV operation (16X reduction in standard deviation).

Standard deviation at 1.3 GeV operation is also reduced, but only by a factor of ~2.7.

SNS corrector multipole 27CDM30

Dipole and Quad windings

Windings for Sextupole

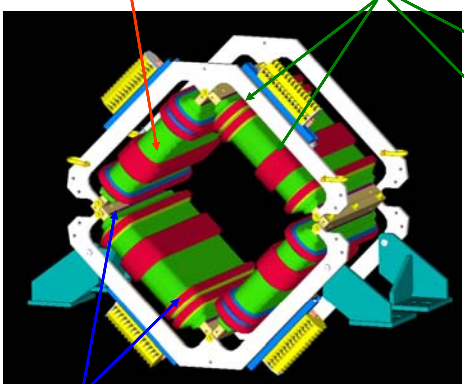

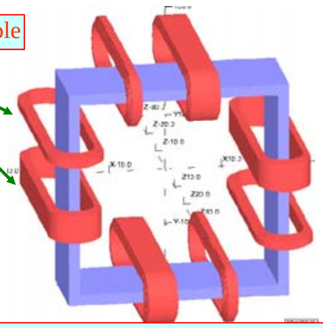

Windings to minimize Sextupole due to dipole

$B_r=b_0 + a_1(r)\cos(3\theta) + a_2(r)\cos(3\theta)$

	dip.	sq_quad	sq_sext
$\int b_0 dz$	8.2	[kGcm]	at r=10 [cm]
$\int a_1(r)dz$	0.27	[kG]	at r=10 [cm]
$\int a_2(r)dz$	0.066	[kGcm^{-1}]	at r=10 [cm]

The sextupole due to dipole minimized:

$\int b_n(r)dz/\int b_0 dz < \pm 2\times10^{-3}$ r=10cm

2.7 Vacuum chamber & shielding

Typical RCS half-cell layout

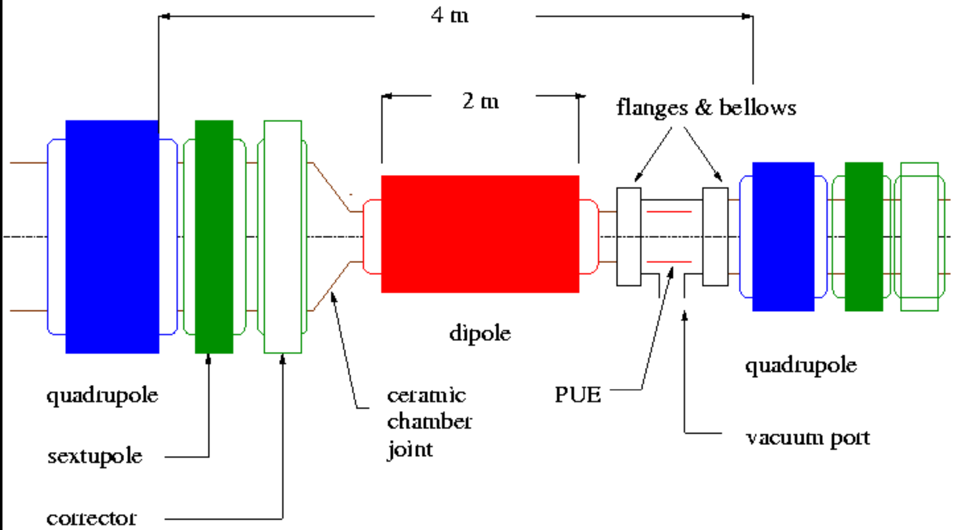

SNS ring vacuum chamber

(electron detector)

J-PARC ceramic vacuum chamber

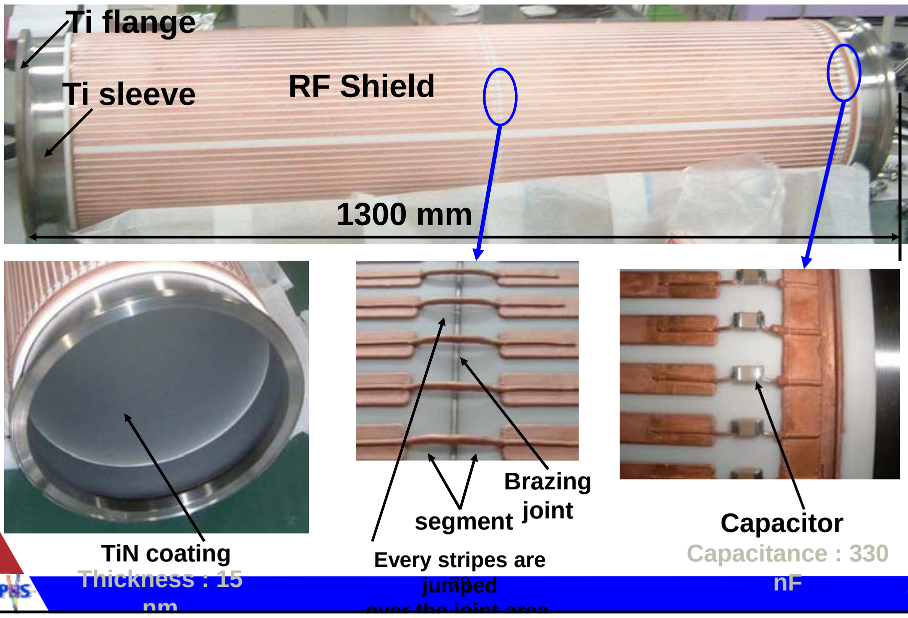

Vacuum considerations

- High repetition rate
  - Eddy current -> ceramic vacuum duct
- Large aperture
  - Engineering difficulties
- Beam coupling impedance
  - RF shielding of beam image current
- Electron cloud suppression
  - Surface coating of TiN

Eddy current effects

- Eddy current induced sextupole field

$$\frac{\partial^2 B_y}{\partial x^2} = \frac{\mu_0}{\rho_r} \frac{d_w}{g} \dot{B}$$

- – Inversely proportional to resistivity, gap height
- – Proportional to ramp rate, chamber width

Leading sources of field imperfections are ramping Eddy-current and saturation. Variation in the level of saturation contributes to the tracking errors between different types of magnet. Eddy-currents induced in the vacuum chamber under the changing magnetic field distort and delay the field and generate multipole errors. For a wide chamber of thickness d_w inside a dipole magnet of gap g, the sextupole field is given by (Edwards , 1993; Rice , 1998)

Thermal heating

Consider a pipe of thickness d_w and volume resistivity ρ_r. As an example, for a resistive loop of width w_r and height h_r penetrated by a magnetic field B, the instantaneous power per unit length is given by

$$\frac{dP_r}{ds} = \frac{\dot{B}^2 w_r^2 h_r d_w}{2\rho_r}. \tag{15}$$

For a circular pipe of radius b, the average power is proportional to the repetition rate, the field-variation rate, the magnetic-field amplitude squared, and the pipe's radius, b, cubed. It also is inversely proportional to the sheet-resistivity ρ_r/d_w.

Vacuum chamber candidates

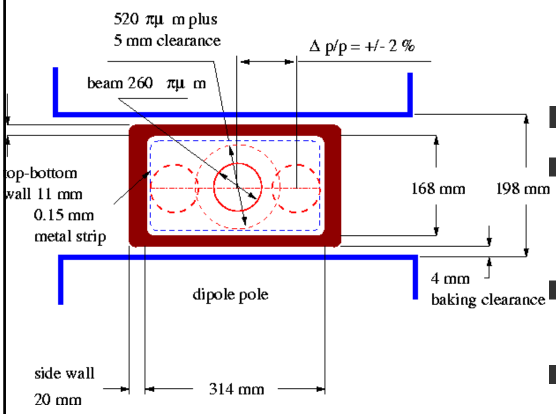

- Conventional:
  - metal pipe
  - connected to magnets (FNAL Booster)
- RCS cadidates:
  - Ceramic chamber w/ sustained shield following beam contour (ISIS)
  - Ceramic w/ printed wires (KAON study, SNS/RCS)
  - Ceramic w/ external shield & internal coating (JKJ)
  - Thin Inconel pipe (FNAL PD)

SNS vacuum chamber example

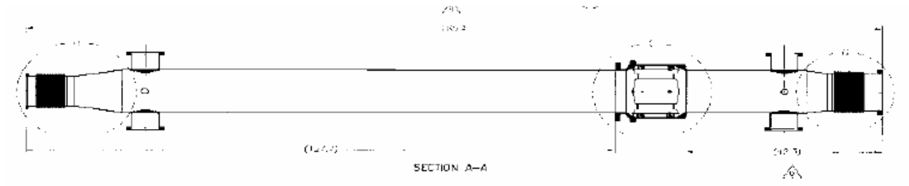

Fig. 2 Schematics of typical SNS ring straight section doublet chambers for 30cm quadrupole doublets.

- Number of vacuum chamber type minimized
- Stainless steel pipe, inconel bellows for radiation resistance
- Inner surface coated with TiN to suppress electron cloud

2.8 Beam diagnostics & machine protection

SNS diagnostics overview

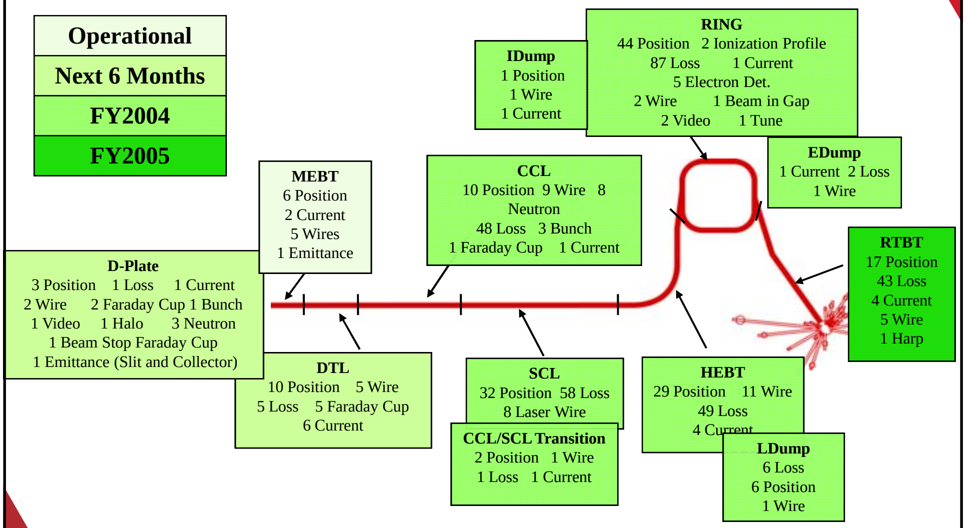

CPNS

85

SNS ring diagnostics

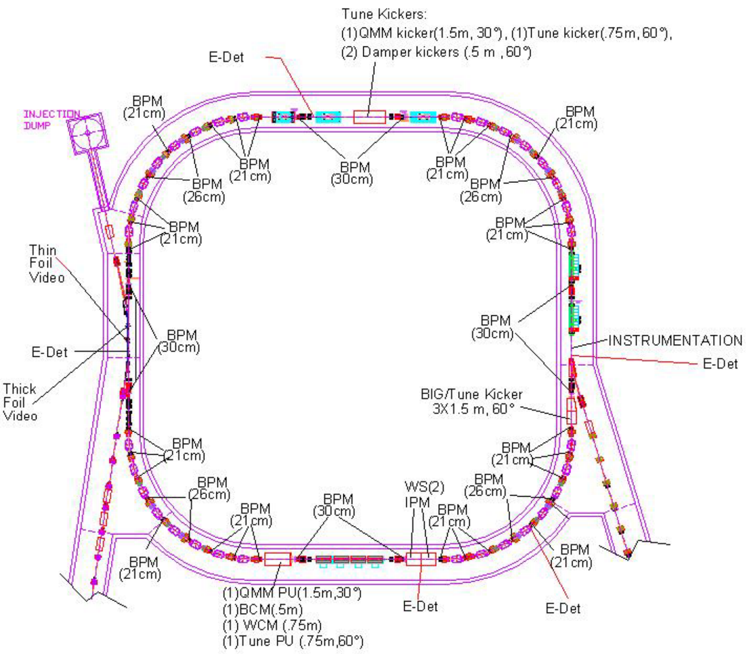

CPNS

86

SNS diagnostics layout example

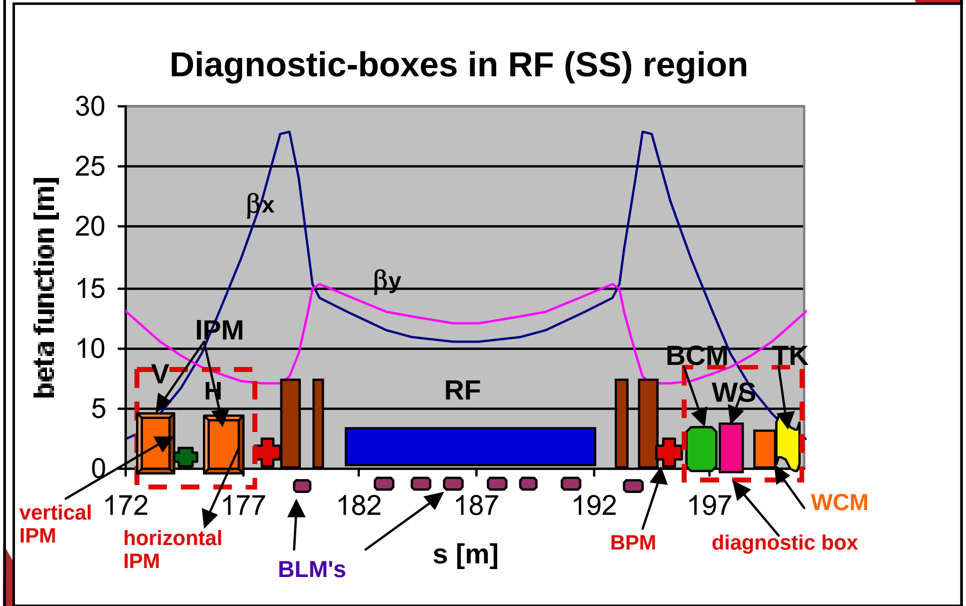

SNS diagnostics requirements table

Ring System Diagnostics AP Requirements (11/2002)

Device	Location	Intensity [ppp]	Range	Accuracy	Resolution	Data structure	Comments
BPM (position)	Ring, HEBT,RTBT	5e10 - 2e14	+/- pipe radius	+/-1%	0.5/1.0%	aver./turn-by-turn	dual plane/high frequency correction for non-linear region average < 1.5e11 402.5MHz
BPM (phase)	HEBT	5e10 - 2e14	+/- 180 deg	+/-2 deg	0.1 deg		
IPM	Ring	5e10 - 2e14	+/- 64mm	2.2mm	2.2 mm	few per turn	H,V; pressure bump early
BLM (0.1 HZ)	Linac-HEBT Ring,RTBT	2e8 - 2e14	1-2.5e5 rem/h 1-2.5e5 rem/h	1%	0.5 r/h	10 s averaging	1% of 1 W/m
BLM (35 kHZ)	Linac-HEBT Ring,RTBT	2e10 - 2e14	1-2.5e5 rem/h 1-2.5e5 rem/h	1%	50 rem/h	at 6Hz rate, sel. 10 BLMs at 10Hz	
FBLM	Linac-HEBT Ring		1-1000 rem/h 1-1000 rem/h			inside mini pulse intra turn	fast; not calibrated
BCM	MEBT-to-HEBT Ring-RTBT	 5e10 - 2e14	15mA - 52 mA 15mA - 100A	1% 1%	.5% .5%	inside mini pulse turn-by-turn	 All are Fast Current Transf.
Tune	Ring			+/- 0.001 +/- 0.005	+/- 0.0005 +/- 0.001	req. averaging req. averaging	tune kicker/pick-up - coherent BTF and QM - incoherent
Wire	HEBT Ring RTBT	5e10 - 2e11 5e10 - 2e14 2e12 - 2e14	+/- pipe radius +/- pipe radius +/- pipe radius	10%rms width 10%rms width 10%rms width	5%rms width 5%rms width 5%rms width	40KHz 40KHz 40KHz	SEM SEM+FBLM SEM+FBLM
Beam-in-gap	Ring		0 - 0.1 A	20%			BIG kicker/mon., relative acc.
Foil Video	Ring	5e10 - 2e14	Visible - near IR	+/- 1mm	+/- 1mm	standard video data	2 systems (primary, secondary), phosphor screen
e - detectors	Ring		2e8 - 2e11 (e-)	5%	1e8 (e-)	turn-by-turn	5 locations: Inj.,Coll., Ext, IPM and in the arc; MCPs?
Luminescence	Ring						vacuum chambers,É

Loss monitor detector types

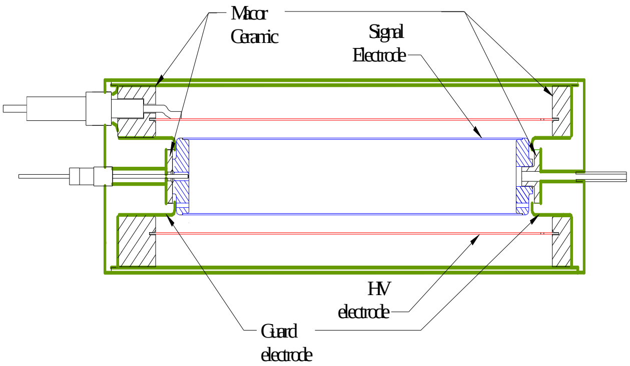

- Ion Chambers
  - Main array
- Neutron Detectors
  - Photo-multipliers
  - In lower energy Linac
  - Provided by INR
- FBLMs
  - For observing sub mini-bunch losses
  - HEBT, Ring, RTBT

Upper end loss limit:	Response up to 0.5 % fast single point (Linac, HEBT), 0.1% in Ring, RTBT
Lower end loss limit:	1% resolution of 1 W/m loss over 10 sec average

Beam Current Monitors

- MEBT to HEBT 0.3 - 1000 us,
  - *15 to 52mA*
  - *Accuracy < 1%*
  - *Resolution 0.5%*
  - *Detail within mini-pulse*

Ring to RTBT 5e10 to 2e14 Protons

- »0.015A to 100A
- »Accuracy < 1%
- »Resolution 0.5%
- »Turn-by-turn data

LOCATION	DIAM.	NUMBER OF BCMS
Front End	5.5cm ID 13.5cm OD	2
Linac	2.5cm,3.0cm,8cm ID	DTL=6 CCL=2 SCL=1
HEBT	13cm ID	5
Ring	22cm ID	1
RTBT	22cm ID	5
	TOTAL	22

BPM processing linearity to displacement

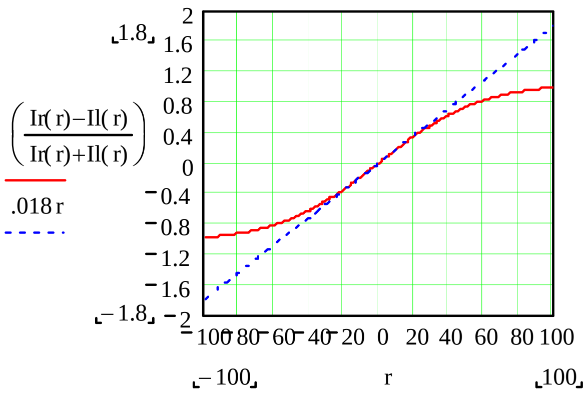

A plot of sensitivity along the axis of a pair of pick-up elements for a 70 degree stripline designed BPM with a half aperture of 105mm. The sensitivity is shown to be 0.018 per mm. Linearity is shown to be "reasonable" over a range of +/- 20mm.

Tune measurements

Coherent tune
accuracy .001
Resolution .0005
Incoherent tune
accuracy .005
Resolution .0025

Hardware used: pulser, kicker, BPM & associated DAQ/processing electronics

Initial processing executed in BPM PCI card

Tune calculations performed in a LabVIEW program

Measured one or more times during accumulation cycle for 1-10 turns

AP required measurement accuracy = +/- 0.001

AP required measurement resolution = +/- 0.0005

Measurement requires averaging

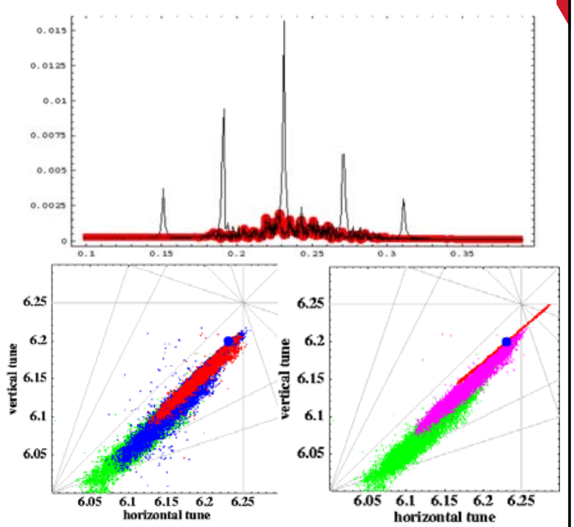

Electron detector

Side View

Top View

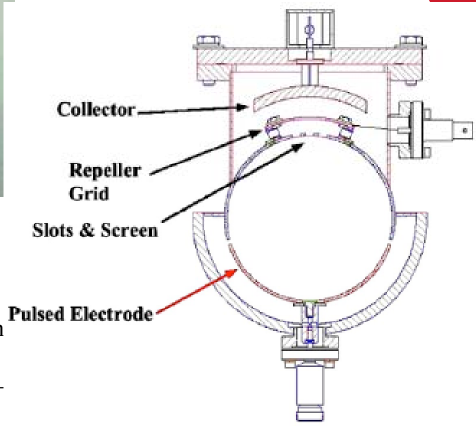

Range:

100pC/cm^2/turn minimum collected current
10nC/cm^2/turn is expected to interfere with beam

We will design for the range, 5x10^{-11}C/cm^2/turn – 10^{-6}C/cm^2/turn

Data Structure:

Digitize at 400MS/s, using standard PCI scope card

SNS video foil monitor

Secondary (thick) Foil Camera Cubby

Primary (thin) Foil Camera Cubby

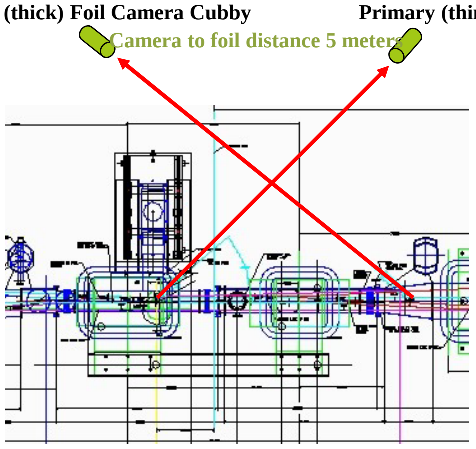

HEBT Beam

Paraffin or boron type neutron shield in cubbies.

Estimated Radiation levels
The main cause of loss at injection will be nuclear scattering at the thin carbon foil.
Uncontrolled loss = 2.5W/m
Produces about 250 R/hr at 1 ft.

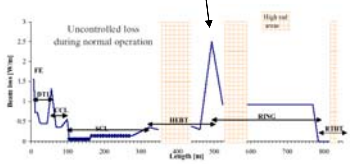

SNS/AP Tech note 7

Est. Camera Dose 10's kR/year

SNS foil monitor video camera assembly

Dage 70RV camera, ND filter, lens assembly on rails inside cubby recessed in nearby wall.

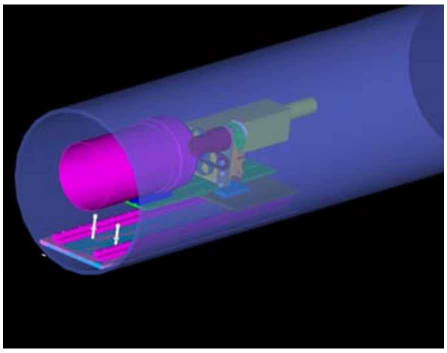

The cubby hole, camera mount, with drawer slides.

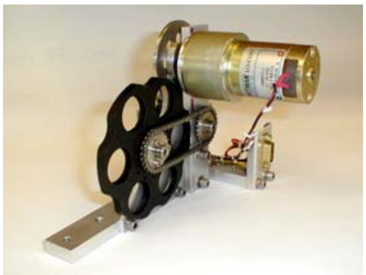

Neutral density filter assembly (C-AD):
DC motor drive
Geneva gear with chain
6 positions (blank, 1, 2, 3, 4, 5)

SNS ionization profile monitor

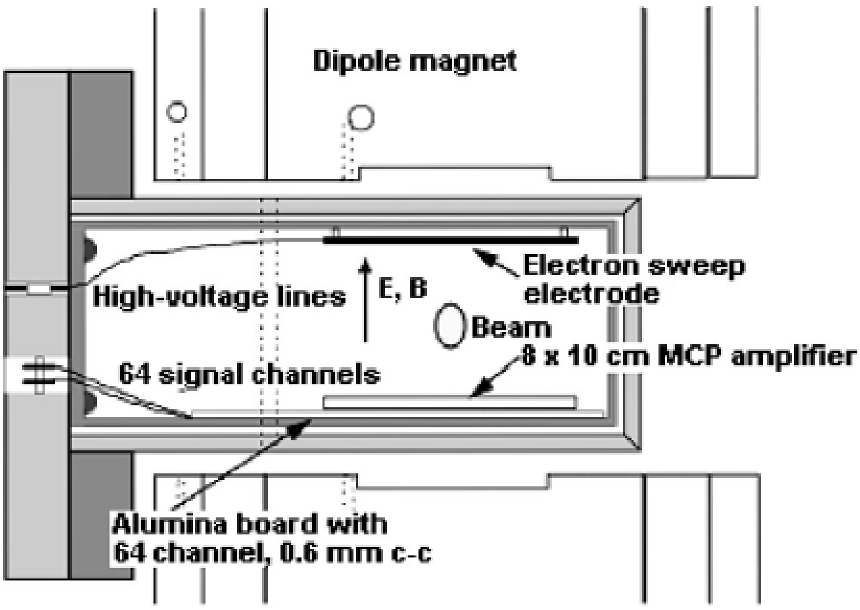

SNS wall current monitor

- **Features**
  - Ferrite-loaded cavity
  - Balanced gap resistors
  - High current handling
- **Measurements**
  - Beam revolution frequency
  - Longitudinal profiles
  - Injection phase error

Wall current monitor profiles

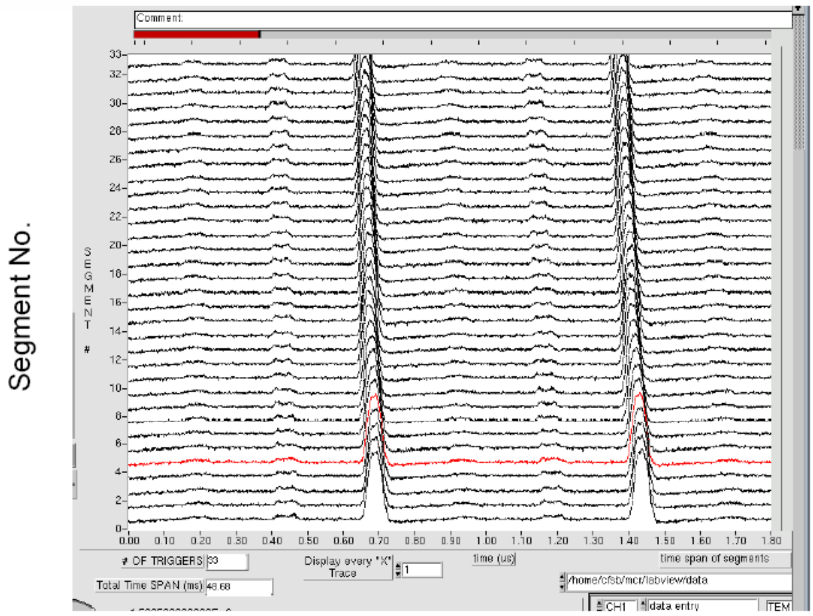

3. Beam dynamics: intensity limiting mechanisms

3.1 Transverse tune shifts & resonances

SNS ring tune diagram

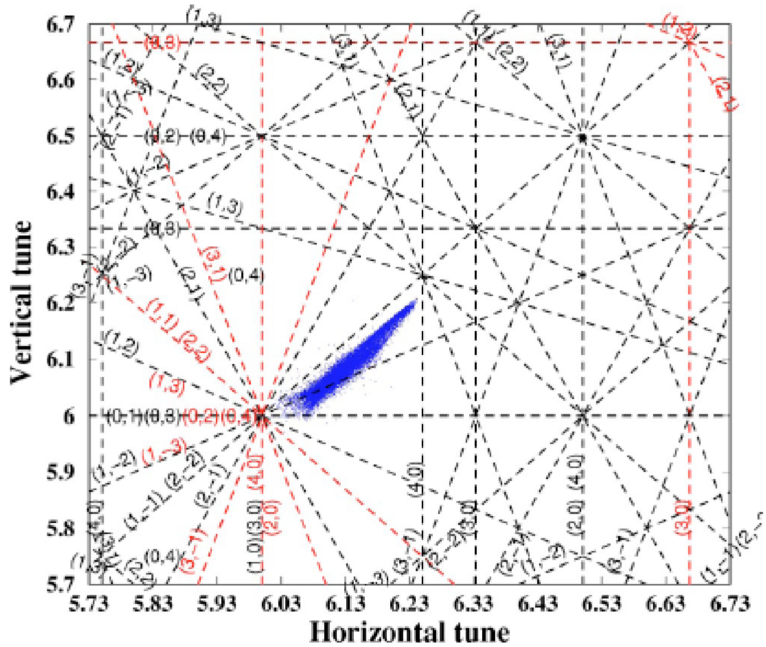

TABLE II. Tune shift produced by various mechanisms on a 2-MW beam in the SNS ring with transverse emittance of 120π μm in each plane and momentum spread of $\pm 0.7\%$ (Sec. IV.A).

Mechanism	Maximum tune shift
Space charge	-0.2 (2 MW beam)
Chromaticity	± 0.06 (0.7% $\Delta p/p$)
Kinematic nonlinearity (480π)	0.001
Fringe field (480π)	± 0.025
Uncompensated ring magnet error (480π)	± 0.02
Compensated ring magnet error (480π)	± 0.002
Fixed injection chicane	± 0.004
Injection painting bump	± 0.001
Electron cloud	~ 0.04

Space charge & chromatic tune shifts

- Transverse tune shift: $$\Delta\nu_{\rm sc} \approx \frac{f_{\rm sc} N_0 r_0}{4\pi B_f \epsilon_{\rm rms} \beta^2\gamma^3}$$

$$\epsilon_{\rm rms} = \sigma_\perp^2/\beta_\perp \qquad \beta_\perp \approx R_0/\nu_0.$$

  - Based on cancellation between electric and magnetic field for relativistic particles
  - Strong dependence on energy

- General Laslett tune shift

$$\Delta\nu_{x,y} = -\frac{f_{\rm sc} N_0 r_0 R_0}{2\pi B_f \nu_{x,y,0}\beta^2\gamma}\left[\frac{1}{\sigma_{x,y}(\sigma_x+\sigma_y)}\left(\frac{1}{\gamma^2}-\eta_e\right)+A_{im}^e\left(\gamma^{-2}-\eta_e\right)+A_{im}^m\right]$$

- Chromatic tune shift $$\Delta\nu_\perp = \xi_\perp \frac{\Delta p}{p},$$

Magnetic imperfections

$$\begin{aligned}\Delta\nu_x = &\left(-\frac{\Delta b_0}{2\rho}+\frac{b_0\delta}{2\rho}-C_1\right)\beta_x+3C_2\beta_x^2\epsilon_x-6C_2\beta_x\beta_y\epsilon_y\\ &+\frac{15}{2}C_3\beta_x^3\epsilon_x^2-45C_3\beta_x^2\beta_y\epsilon_x\epsilon_y+\frac{45}{2}C_3\beta_x\beta_y^2\epsilon_y^2\\ &+\frac{35}{2}C_4\beta_x^4\epsilon_x^3-210C_4\beta_x^3\beta_y\epsilon_x^2\epsilon_y+315C_4\beta_x^2\beta_y^2\epsilon_x\epsilon_y^2\\ &-70C_4\beta_x\beta_y^3\epsilon_y^3+\frac{315}{8}C_5\beta_x^5\epsilon_x^4-\frac{1575}{2}C_5\beta_x^4\beta_y\epsilon_x^3\epsilon_y\\ &+\frac{4725}{2}C_5\beta_x^3\beta_y^2\epsilon_x^2\epsilon_y^2-1575C_5\beta_x^2\beta_y^3\epsilon_x\epsilon_y^3\\ &+\frac{1575}{8}C_5\beta_x\beta_y^4\epsilon_y^4, \end{aligned} \tag{24}$$

$$\begin{aligned} C_1 &= \frac{1}{2}(\Delta b_1 - b_1\delta)+b_2\Delta_x-a_2\Delta_y+\frac{3}{2}(b_3\Delta_x^2-a_3\Delta_y^2),\\ C_2 &= \frac{1}{2}\left(\frac{1}{4}b_3+b_4\Delta_x-a_4\Delta_y\right),\\ C_3 &= \frac{1}{4}\left(\frac{1}{6}b_5+b_6\Delta_x-a_6\Delta_y\right),\\ C_4 &= \frac{1}{8}\left(\frac{1}{8}b_7+b_8\Delta_x-a_8\Delta_y\right),\\ C_5 &= \frac{1}{16}\left(\frac{1}{10}b_9+b_{10}\Delta_x-a_{10}\Delta_y\right), \end{aligned} \tag{26}$$

and

$$\Delta_x = D_x\frac{\Delta p}{p}+x_c, \quad \Delta_y = D_y\frac{\Delta p}{p}+y_c. \tag{27}$$

- Tune shifts and action kicks due to magnetic imperfections characterizes the impacts

Combined tune spread: various intensities

w.p. (6.23,6.20) – combined tune spreads at the end of accumulation:

N=0.1*10[14] - red

(mainly chromatic spread and resulting loss due to resonances above- chromaticity correction with sextupoles or slight w.p. adjustment)

N=1*10[14] - pink

(depressed by space charge)

N=2*10[14] - green

(depressed by space charge)

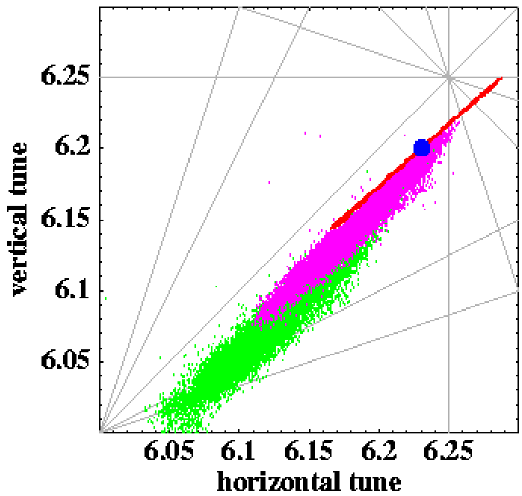

Resonance condition

- Resonance condition: $m\nu_x + n\nu_y = k,$
  - resonance order $l = |m| + |n|.$
- Structure resonance: k is an integral multiple of the lattice periodicity
- Resonance stop band width:

$$\Delta\nu^{(m,n)} = \pm|\kappa|\epsilon_x^{|m|/2}\epsilon_y^{|n|/2}\left(\frac{m^2}{\epsilon_x} + \frac{n^2}{\epsilon_y}\right).$$

  - resonance strength

$$\kappa = \frac{R_0}{\pi 2^l m! n!}\oint \beta_x^{|m/2|}\beta_y^{|n/2|}K_\perp^{(l)}\exp(i\Psi)\,d\theta, \qquad K_\perp^{(l)} = \frac{1}{B_0\rho}\left(\frac{\partial^{(l-1)}B_i}{\partial x^{(l-1)}}\right),$$

3.2 Beam loss mechanisms

SNS estimated controlled beam loss

TABLE III. Estimated controlled loss of a proton beam at 1 GeV in the SNS ring, linac-to-ring transport (HEBT), and ring-to-target transport (RTBT) (Sec. IV.B.1). Losses are given as a fraction of the total beam intensity. The total beam power is 2 MW.

Mechanism	Location	Fraction	Power
HEBT:			
H^0 from linac	linac dump	10^{-5}	20 W
linac transverse tail	HEBT H/V collimator	10^{-3}	2 kW
energy jitter/spread from linac	HEBT L collimator	10^{-3}	2 kW
Ring:			
beam-in-gap	BIG kicker/collimator	10^{-4}	200 W
excited H^0 at foil	collimator	1.3×10^{-5}	26 W
partial ionization at foil	injection dump	10^{-2}	20 kW
foil miss	injection dump	10^{-2}	20 kW
ring beam halo	collimator	1.9×10^{-3}	3.8 kW
energy straggling at foil	collimator	3×10^{-6}	6 W
RTBT:			
kicker misfiring	RTBT collimator	10^{-5}	20 W

SNS estimated uncontrolled beam loss

TABLE IV. Estimated uncontrolled loss of a proton beam at 1 GeV in the SNS ring, linac-to-ring transport (HEBT), and ring-to-target transport (RTBT) (Sec. IV.B.2). Losses are given as a fraction of the total beam intensity distributed in the specified machine length. The total beam power is 2 MW.

Mechanism	Location	Fraction	Length (m)	Power (W/m)
HEBT:				
H^- magnetic stripping	all HEBT	1.7×10^{-6}	169	0.02
collimator outscattering	HEBT achromat	7.5×10^{-6}	15	0.1
Ring:				
H^- magnetic stripping	injection dipole	1.3×10^{-7}	1	0.3
nuclear scattering at foil	foil	3.7×10^{-5}	30	2.5
collimation inefficiency	all ring	10^{-4}	218	0.9
RTBT:				
nuclear scattering at window	target window	4×10^{-2}		

Resonance loss model (SNS ring simulation)

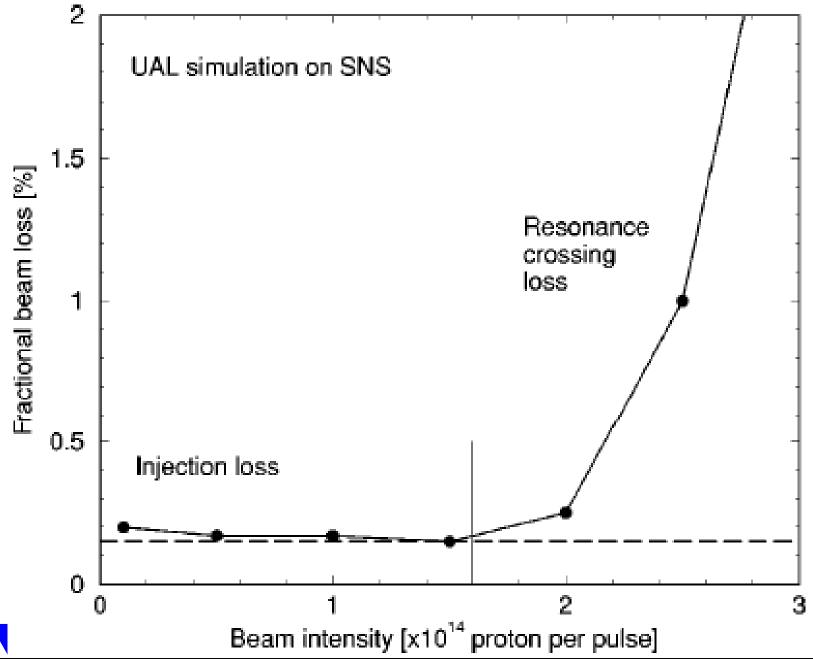

Measured uncontrolled beam loss at the PSR

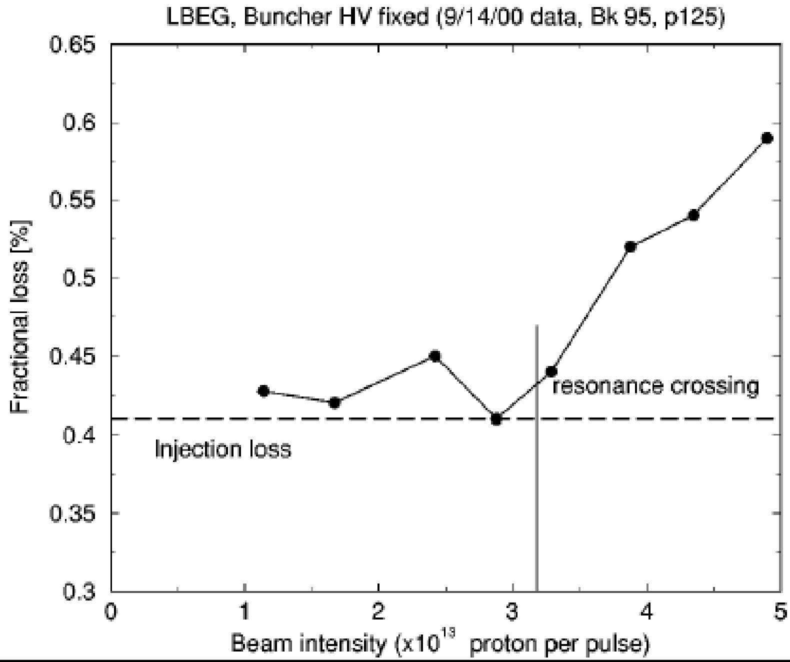

3.3 Collective effects

Space charge & halo formation

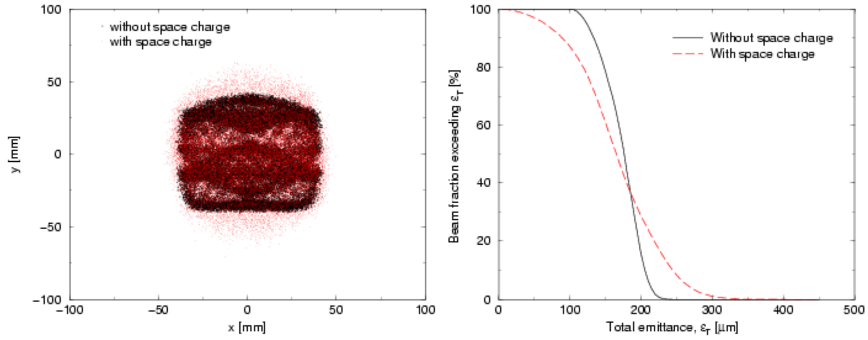

FIG. 41 Vertical emittance growth due to space charge if anti-correlated painting is used during SNS beam accumulation. The transverse tunes are (6.23, 6.20). For the data shown in black, space-charge was neglected; for the data shown in red, the space-charge force for a 2 MW beam was included. Space charge produces a significant beam tail (Section IV.C.1, courtesy A. Fedotov).

Beam tail from space charge & field error

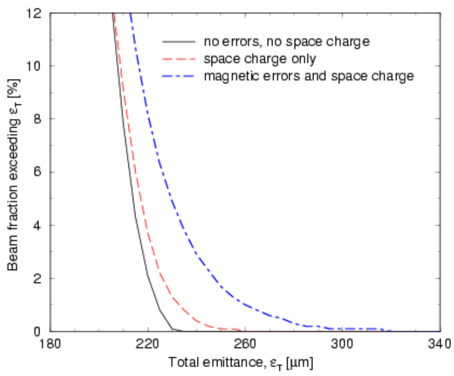

FIG. 42 Beam tail driven by space charge and magnet errors. The development of beam tail is noticeably enhanced by the combination of these two driving sources (Section IV.C.1). A non-standard working point, (6.40, 6.30), is chosen to illustrate the effect. The noimnal working point, (6.23, 6.20), is chosen to avoid resonances that lead to the development of such enhanced beam tail (Section IV.C.1, courtesy A. Fedotov).

Beam coupling impedance

TABLE V. Estimated beam coupling impedance of the SNS accumulator ring at frequency below 10 MHz. The beam revolution frequency is 1.058 MHz. The leading impedance source contributing to possible instability is the extraction kicker modules located inside the beam vacuum pipe (Sec. IV.C.2).

Device/Mechanism	$Z_\parallel/n$ (Ω)	$Z_\perp$ (kΩ/m)	Comment
Space charge	$-j196$	$j(-5.8+0.45)\times 10^3$	incoherent and coherent part
Extraction kicker	$0.6n+j50$	$33+j125$	25 Ω termination at PFN
Injection kicker & pipe	$0.5/n$	17.5	pipe coated; lowest tune at 200 Hz
Injection foil assembly	$j0.05$	$j4.5$	MAFIA modeling
rf cavity	0.9 (resonance peak)	18	to be damped
Resistive wall	$(j+1)0.71$ at ω_0	$(j+1)8.5$ at ω_0	
Broadband beam position monitor	$j4$	$j18$	
Broadband bellows	$j1.1$	$j7$	unscreened
Broadband steps	$j1.9$	$j16$	tapered 1-to-3 ratio
Broadband ports	$j0.49$	$j4.4$	screend
Broadband valves	$j0.15$	$j1.4$	unscreened
Broadband collimator	$j0.22$	$j2.0$	

CPHS

Space charge impedances

$$Z_{\|}^{\rm sc}(\omega) = -j\frac{n g_0 Z_0}{2\beta\gamma^2}; \quad Z_{\perp}^{\rm sc}(\omega) = -j\frac{g_0 Z_0}{\beta^2\gamma^2}\left(\frac{1}{a^2}-\frac{1}{b^2}\right)$$

$$n = \omega/\omega_s,\ Z_0 = (\varepsilon_0 c)^{-1} = 377\ \Omega \qquad g_0 \approx 1/2 + 2\ln(b/a)$$

- Longitudinal
  - Defocuses the beam longitudinally (below transition)
  - Capacitive
  - Cancellation between electric and magnetic forces results in strong energy dependence
- Transverse
  - Strong dependence on energy
  - Strong dependence on vacuum chamber size
  - ISIS: wire cage tapered according to beam envelope

CPHS

Resistive wall impedance

- Resistive wall impedance

$$Z_{\parallel}^{\text{rw}}(n\omega_s) = n(1+j)\frac{\beta Z_0 \delta_s}{2b}; \quad Z_{\perp}^{\text{rw}}(n\omega_s) = (1+j)\frac{R_0 Z_0 \delta_s}{b^3}$$

- Skin depth

$$\delta_s = \sqrt{\frac{2\rho_r}{\mu\omega}}$$

  - Larger radius vacuum chamber is preferred
  - Image passage thought RF shielding with thickness larger than the skin depth
  - Conductive coating with thickness thinner than skin depth is often used; complicated analysis

Extraction kicker impedance iterations

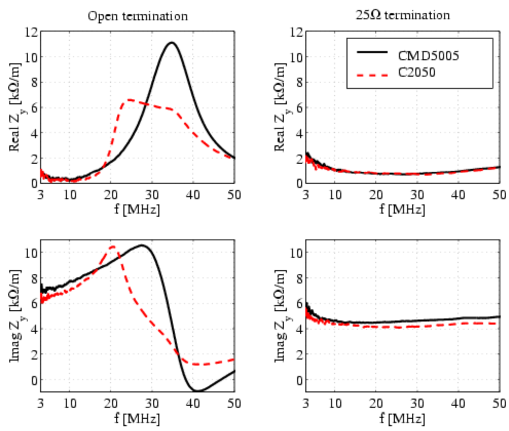

FIG. 43 Comparison of bench-measured coupling impedance for open and 25 Ω PFN termination, and high (1600) and medium (100) permeability ferrite of the SNS ring extraction-kicker assembly. The extraction kickers, residing inside the vacuum chamber of the SNS ring, are a major source of beam-coupling impedances (Section IV.C.2, courtesy D. Davino and H. Hahn).

Instabilities

TABLE VI. Collective effects and estimated thresholds for a 2-MW beam power in the SNS accumulator ring. The dominant effects are expected to be beam halo and beam loss generated by space-charge-related resonance crossing. Other intensity-limiting mechanisms include electron-cloud effects and instabilities due to the extraction kicker coupling impedance (Sec. IV.C.3).

Mechanism	Threshold	Comments
Transverse space charge	$\Delta\nu_{sc} \approx -0.2$	resonance crossing
Longitudinal space charge	15 kV induced RF voltage	60 kV RF voltage
Transverse microwave instability	$Z_\perp \approx 60$ kΩ/m	extraction kicker impedance
Longitudinal microwave instability	$\lvert Z_\parallel/n \rvert \approx 100$ Ω	extraction kicker impedance
Resistive wall		(walls and kicker impedance)
(ξ=0)	$Z_\perp \approx 1.3$ kΩ/m	at 200 kHz; rise time >300 μs
(ξ=−3)	$Z_\perp \approx 100$ kΩ/m	at 200 kHz
Electron cloud	above 2 nC/m	above 2% neutralization in beam

3.4 Electron cloud effects

Electron-cloud phenomena: PSR

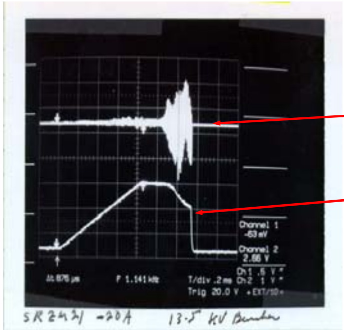

Instability signals

BPM ΔV signal

CM42 (4.2 μC) (Circulating Beam Current)

- Growth time ~ 75 μs or ~200 turns
- High frequency ~ 70 – 200 MHz
- Controlled primarily by rf buncher voltage
- Requires electron neutralization of ~ 1% (from centroid model)

Control by rf buncher voltage

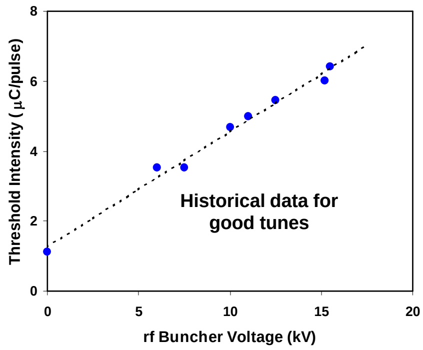

Electron generation

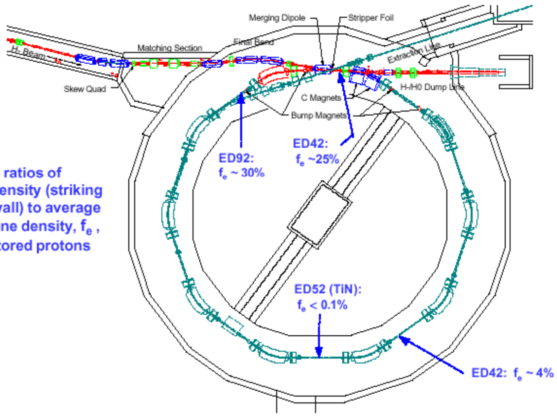

Shown are the ratios of electron line density (striking the chamber wall) to average proton beam line density, f_e, for 5.5 μC of stored protons

PSR e-flux measure

- High electron concentration near injection & extraction
- Electron wall-striking level to be distinguished from electron neutralization level in the bunch

- Major sources of electrons in a high-intensity ring
  - From stripping foil (H^-, H^0)
  - Proton striking collimators or aperture bottleneck
  - Gas ionization, ion desorption, electron desorption
  - Beam-induced electron multipacting

Trailing-edge electron multipacting

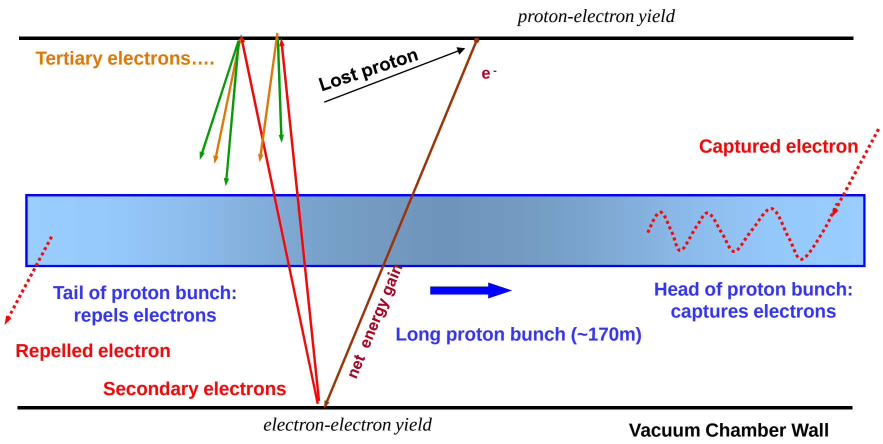

Effects of electron clouds

- Electron neutralization, tune shifts, and resonance crossing
- Transverse (horizontal or vertical) instability
- Associated emittance growth and beam loss
- Vacuum pressure rise
- Heating & damage of vacuum chamber
- Interferences with diagnostics system

Electrons from collimator surface

(courtesy H. Ludewig, N. Simos)

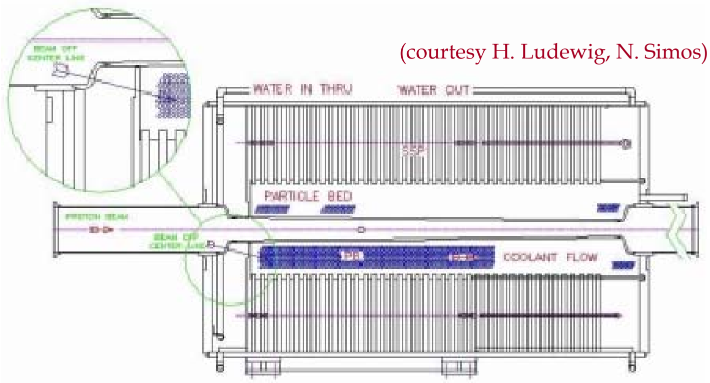

- Designed to absorb 2 – 10 kW (0.1% -- 0.5%) proton beam loss
- Beam halo at large grazing angle enhances electron production
- Possible saw-tooth surface complicated by proton stopping distance
- Possible magnetized surface proposed at LANL
- Rely on two-stage collimation for a large impact distance

Secondary electron yield vs. primary electron energy

(courtesy N. Hilleret, O. Grobner,)

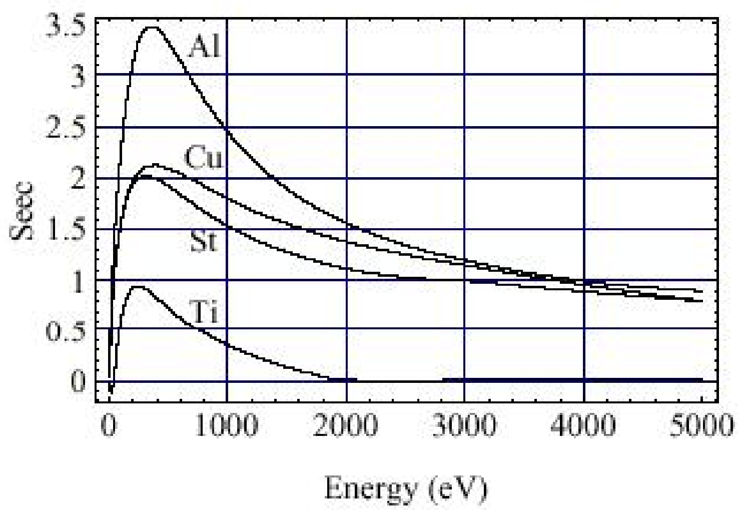

PSR wall-electron spectrum

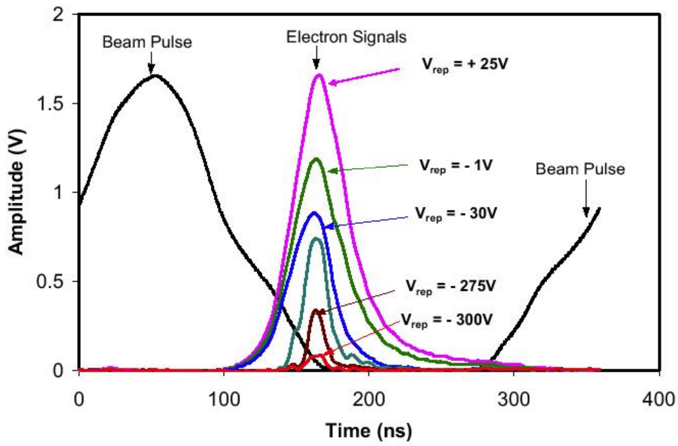

- Trailing-edge multipacting
- Total electrons striking the wall is ~ 25% of the proton number
- Actual neutralization level much lower (swept electron)

Preventive measures

- Suppress electron production
  - Tapered magnets for electron collection near injection foil; back-scattering prevention
  - TiN coated vacuum chamber to reduce multipacting
  - Striped coating of extraction kicker ferrite (TiN)
  - Beam-in-gap kicker to keep a clean beam gap (10^{-4})
  - Good vacuum ($5x10^{-9}$ Torr or better)
  - ports screening, step tapering; BPMs as clearing electrodes
  - Install electron detectors around the ring
  - Two-stage collimation; winding solenoids in the straight section
- Enhance Landau damping
  - Large momentum acceptance with sextupole families; high RF voltage; momentum painting
  - Inductive inserts to compensate space charge
  - Reserve space for possible wide band damper system

Electron-cloud mitigation

- Inner surface of vacuum chambers coated with TiN to reduce secondary electron emission
- Solenoids used in collimation region to confine scattered electrons
- Beam-position-monitors act as clearing electrodes
- Beam-in-gap kicker to clear residuals
- Extra vacuum ports for beam scrubbing

(Courtesy H. Hseuh, P. He, M. Blaskiewicz, L. Wang, SY Zhang et al)

SEY= 2.4, as-received condition

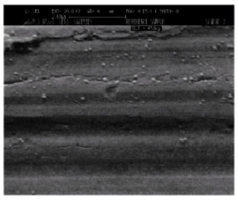

FIG. 8. Secondary electron image of copper as-received (magnification = 15 000).

SEY= 1.1 after air and vacuum bake

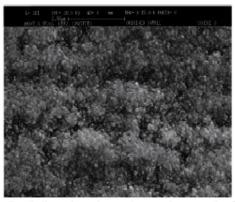

FIG. 9. Secondary electron image of copper after 5 min air exposure at 350 and 350 °C bakeout under vacuum (magnification = 15 000).

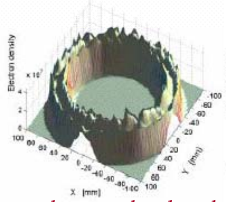

electron cloud under a solenoid

electron cloud under a clearing electrode

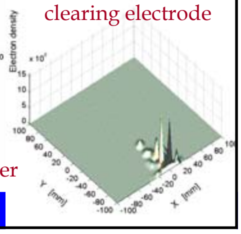

Ring vacuum chamber coating

(Hseuh, He, Todd …)

Injection kicker ceramic chamber double coating

Cu (~ 0.7 μm) for image current

TiN (0.1 μm) for electron cloud

Meets requirement: conductive coatings w/ end-to-end resistance of ~0.04Ω ± 50% (Henderson, Davino)

Thickness uniformity < ± 30%

Extraction kicker ferrite patterned TiN coating

0.1 μm TiN on ≥ 90% inner surface, with good adhesion

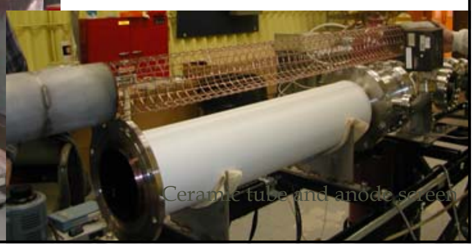

Solenoid effects (*L. Wang, M. Blaskiewicz, et al*)

- 30G Solenoid field can reduce the e-cloud density with a factor 2000 !
- Zero density within beam
- Solenoid winding in the collimator straight section

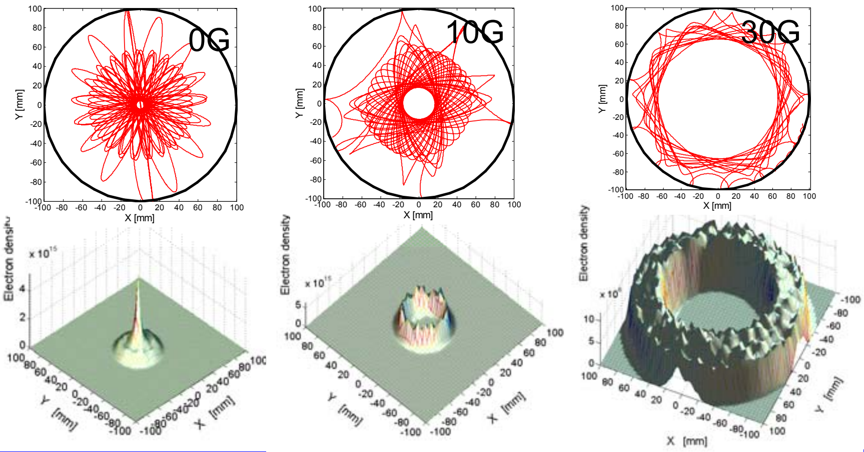

3.5 Computer simulation codes

Simulation codes

TABLE VIII. Examples of beam dynamics simulation codes and their functions used for the design of high-intensity circular accelerators (Sec. IV.F). Courtesy N. Malitsky.

Functions	UAL	ORBIT	FTPOT	MAD	MARYLIE	ACCSIM	SIMPSONS
Interface	**PERL API**	**SuperCode**	**FTPOT**	**MAD**	**MARYLIE**	**ACCSIM**	**SIMPSONS**
MAD elements	Yes	Yes	Yes	Yes	Yes	Yes	Yes
Errors	Yes	No	Yes	Yes	No	No	Yes
Tracking	Thin lenses	Matrices + nodes	Thin lenses	Lie algebra	Lie algebra	Matrices + nodes	Thin lenses
Mapping	Any order	Second order	Second order	Third order	Third order	Linear order	No
H Painting	Yes	Yes	No	No	No	Yes	Yes
Fringe Field	Yes (Maps)	No	No	No	Yes	No	No
Space Charge	3D	3D	No	No	No	2.5D	2D & 3D
Analysis (twiss ...)	Yes	No	Yes	Yes	Yes	No	No
Optimization (lattice ...)	No	No	No	Yes	Yes	No	No
Correction (orbit ...)	Yes	No	Yes	Yes	Some	No	No
Impedance	Yes	Yes	No	No	No	No	No
Collimator	Yes	Yes	No	No	No	Yes	No
Integration of lattices	Yes	No	No	No	No	No	No

4. Future applications & developments

TABLE IX. Beam parameters of some existing and proposed proton accelerator facilities (Sec. V); RCS, rapid-cycling synchrotron; AR, accumulator ring; EA, energy amplifier; PD, proton driver; Linac, linear accelerator.

Machine	Intensity (10^{13}/pulse)	Rep. rate (Hz)	Flux[a] (10^{20}/year)	Energy (GeV)	Power (MW)	Type
Existing:						
ISIS (RAL)	2.5	50	125	0.8	0.16	RCS
AGS (BNL)	7	0.5	3.5	24	0.13	RCS
PSR (LANL)	2.5	20	50	0.8	0.064	AR
MiniBooNE (FNAL)[b]	0.5	7.5	3.8	8	0.05	RCS
NuMI (FNAL)	3	0.5	1.5	120	0.3	RCS
CNGS (CERN)	4.8	0.17	0.8	400	0.5	RCS
Under construction:						
SNS	14	60	840	1	1.4	AR
J-PARC 3 GeV	8	25	200	3	1	RCS
J-PARC 50 GeV	32	0.3	10	50	0.75	RCS
Proposed:						
ESS	46.8	50	2340	1.334	5	AR (2 ring)
CONCERT	234	50	12000	1.334	25	AR (2 ring)
AAA (LANL)		cw	62500	1	100	Linac
AHF (LANL)	3	0.04	0.03	50	0.003	RCS
EA (CERN)		cw	12500	1	20	Cyclotron
PD (FNAL) I	3	15	45	16	1.2	RCS
PD (FNAL) II	10	15	150	16	4	RCS
PD (BNL) I	10	2.5	25	24	1	RCS
PD (BNL) II	20	5	100	24	4	RCS
PD/SPL (CERN)	23	50	1100	2.2	4	AR (2 ring)
PD (RAL) 15 GeV	6.6	25	165	15	4	RCS (2 ring)
PD (RAL) 5 GeV	10	50	500	5	4	RCS (2 ring)

[a]1 year is taken to be 10^7 s.

[b]Including planned improvements.

未来强子装置设想（黄线框：1000米x100米；150亩）

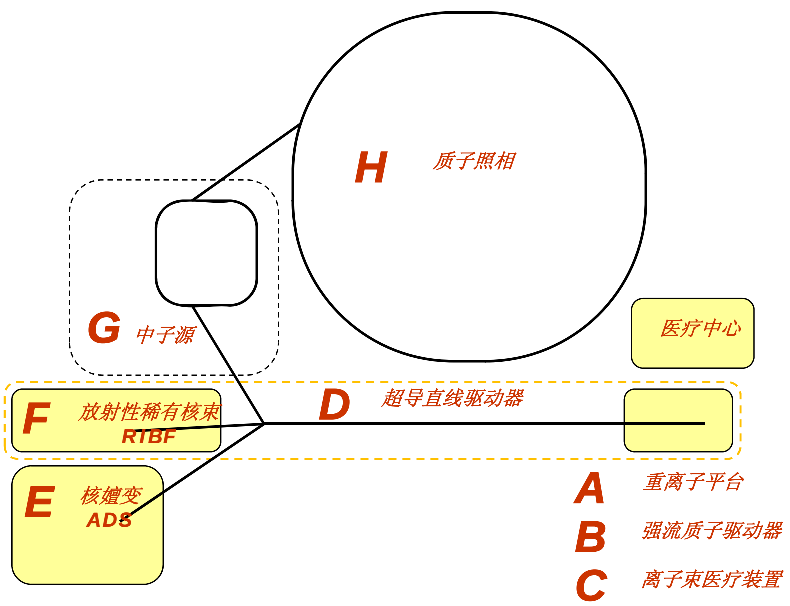

CPNS

136

A possible layout of 10,000 m^2 building

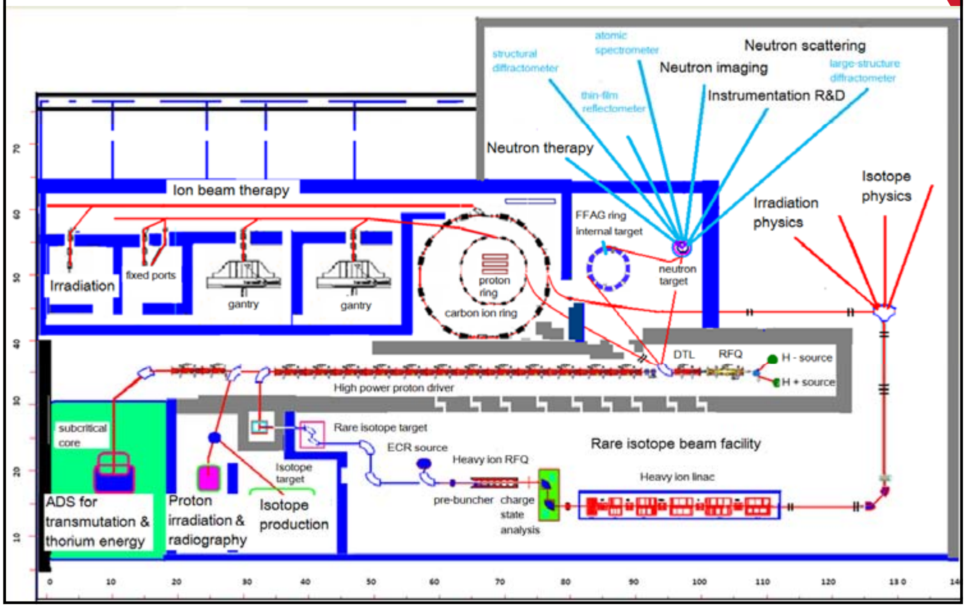

Class references

- J. Wei, Reviews of Modern Physics, Vol. 75 (2003) 1383 – 1432
- **2001** US Particle Accelerator School, “Physics and design of high intensity circulator accelerators”, Colorado, USA
- **2004**: US Particle Accelerator School, “The Spallation Neutron Source II: ring and transports”, Wisconsin, USA
- Handbook of Accelerator Physics and Engineering, A.W. Chao & M. Tigner

Problem 1

- Two identical, vertically stacked rapid-cycling synchrotrons are housed in the same tunnel. The circumference is 300 m. The proton beams are injected at 400 MeV, and extracted at 2 GeV. The repetition rate is 30 Hz for each ring. The pulse in each ring contains 10^{14} particles. The RF system operates at harmonic h=2, and that the pulse contains two bunches.
  - What is the total output beam power? What is the total average current of the facility?
  - What is the tolerable fractional uncontrolled beam loss in each ring?
  - What is the range of RF frequency swing?
  - The beam gap reserved for extraction kicker rise is a minimum 200 ns. Assuming that the bunch density distribution is parabolic. What is the maximum bunching factor? What is the average and peak current in the ring?

Problem 2

- Let E be the total energy, E_k be the kinetic energy, and p be the momentum. Assume that the deviation in kinetic energy is much smaller than the kinetic energy. Prove that

$$\frac{\Delta E}{E} \approx \beta^2 \frac{\Delta p}{p} \qquad\qquad \frac{\Delta p}{p} \approx \frac{\gamma}{1+\gamma}\frac{\Delta E_k}{E_k}$$

where β and γ are the relativistic factors. For a proton beam of 1 GeV kinetic energy with a +/-1% spread in $\Delta p/p$, how accurate are these relations?

Problem 3

- A ring consists of 4 bending arcs, each a horizontal achromat consisting of 4 identical FODO cells of $\pi/2$ phase advance. The dispersion is suppressed. Evaluate the value and location of peak dispersion of the ring in terms of cell length, and compare it with the minimum achievable peak dispersion of a matched FODO cell.
- Repeat this exercise by flipping the polarity or the quadrupoles, i.e. DOFO instead of FODO.
- Replace the dispersion suppression method by the missing-dipole (half-field) scheme. Evaluate the minimum achievable peak dispersion in terms of cell length.
- Compare the advantage and disadvantage of the above three schemes

Problem 4

1) Assume that the betatron phase advance from location s_1 to s_2 is $\Delta\mu$. Prove that the transfer matrix for (x,x') can be written as:

$$M(s_2 \mid s_1) = \begin{bmatrix} \sqrt{\frac{\beta_2}{\beta_1}}(\cos\Delta\mu + \alpha_1 \sin\Delta\mu) & \sqrt{\beta_1\beta_2}\sin\Delta\mu \\ -\frac{1}{\sqrt{\beta_1\beta_2}}\left[(1+\alpha_1\alpha_2)\sin\Delta\mu + (\alpha_2-\alpha_1)\cos\Delta\mu\right] & \sqrt{\frac{\beta_1}{\beta_2}}(\cos\Delta\mu - \alpha_2\sin\Delta\mu) \end{bmatrix}$$

2) Using the result of 1), prove that the condition for realizing a closed orbit bump from s_1 to s_3 using three dipole magnets is

$$\frac{\theta_1\sqrt{\beta_1}}{\sin(\Delta\mu_{32})} = \frac{\theta_2\sqrt{\beta_2}}{\sin(\Delta\mu_{13})} = \frac{\theta_3\sqrt{\beta_3}}{\sin(\Delta\mu_{21})}$$

Here, θ_i is the dipole kick at location s_i, $\Delta\mu_{ij}$ is the phase advance between s_i and s_j.

Problem 5

- Prove that in terms of variable $\mu(s)=\int^{s}\frac{ds'}{\beta(s')}$, the normalized displacement $X\equiv\frac{x}{\sqrt{\beta_x}}$ obeys simply harmonic motion
- With two-stage betatron betatron collimation consisting of a scraper and two collectors, prove that when the conditions

  $$\mu_1=\cos^{-1}\left(\frac{A}{A+H}\right) \qquad \mu_2=\pi-\mu_1$$

  are satisfied, minimum number of secondary particles escape the collimation process. Here, the scraper radius A and the collector radius A+H are both defined in terms of the normalized variables
- Express the above phase-advance conditions in terms of the physical apertures

Problem 6

- Consider beam density distribution in the normalized phase space during multi-turn injection. Define $\rho^2\equiv X^2+X'^2$ and the quantity $\lambda(\rho)\rho d\rho$ is the number of particle populated within the phase-space circle of radius ρ and width dρ.
  - What is the closed-orbit function with time to realize a uniform distribution in phase space with a constant density $\lambda(\rho)$ within a radius R during a total injection time of $t_{\max}$?
  - Prove that the closed-orbit function to realize a Gaussian distribution

    $$\lambda(\rho)=\frac{2N_0}{\sigma^2}\exp\left(-\frac{\rho^2}{2\sigma^2}\right)$$

    is approximately $X_C(t)=\sqrt{2}\sigma\sqrt{-\ln\left(1-t/t_{\max}\right)}$

    where the injection is performed during a time $0<t<t_{\max}$

Problem 7

- Upon multi-turn injection of a beam with emittance ε_i, and Courant-Snyder parameters β_i and α_i, injecting with input beam center $(\bar{x}, \bar{x}')$ relative to instantaneous injection orbit bump. The ring beam emittance is ε, and ring Courant-Snyder parameters β and α at injection.
  – Prove that in the normalized phase space of the ring

$$X \equiv \frac{x}{\sqrt{\beta}} \qquad X' \equiv \frac{dX}{d\mu} = \frac{\alpha x + \beta x'}{\sqrt{\beta}}$$

the injecting beam ellipse becomes upright and the injection position is optimized when

$$\frac{\alpha_i}{\beta_i} = \frac{\alpha}{\beta} = -\frac{\bar{x}'}{\bar{x}}$$

the injecting beam ellipse can be described as

$$\frac{\beta_i}{\beta} X'^2 + \frac{\beta}{\beta_i} X^2 \le \varepsilon_i$$

Problem 7 (continue)

– Let X_C be the injection closed orbit center relative to ring beam origin in the normalized phase space of the ring. The ring emittance circle corresponding to the injecting beam ellipse can be parameterized as

$$\varepsilon(\theta) = \left(X_C + \sqrt{\frac{\beta_i}{\beta}\varepsilon_i} \cos\theta \right)^2 + \frac{\beta}{\beta_i}\varepsilon_i \sin^2\theta$$

Assume that $\varepsilon_i << \varepsilon$

show that when the condition

$$\frac{\beta_i}{\beta} \approx \left(\frac{\varepsilon_i}{\varepsilon}\right)^{1/3}$$

is satisfied, the injecting beam ellipses will all be contained by the emittance circle $\varepsilon(\theta = 0)$ (i.e. minimum phase-space dilution after injection), while the width of the injecting beam is minimum.

Problem 8

- Prove that for a quadrupole magnet, the magnetic errors that are allowed by the quadrupole symmetry are quadrupole, 12-pole, 20-pole, and so on.

Problem 9

- A C-dipole magnet is designed to operate at a field of 1 T. The magnet has a width of 0.8 m, height 0.6 m. The iron material has a relative permeability of 2500. The gap height is 18 cm. The maximum current is 5000 Amp. How many turns of coil is needed for the top and bottom pole?

Problem 10

- A H^- beam of 1 GeV kinetic energy is transported through an achromat of 90 degree bend before the ring injection. Suppose that the magnetic stripping loss criteria is for the fractional beam loss to be below 10^{-7} per meter. Use the following mean decay path length (in meters in the laboratory frame)

$$\lambda_s = \frac{A_{s1}}{B} \exp \frac{A_{s2}}{\beta\gamma B}, \qquad A_{s1} = (2.47 \pm 0.09) \times 10^{-6} \text{ Tm, and } A_{s2} = 15.0 \pm 0.03 \text{ T}$$

  – Estimate the maximum magnetic field that can be used to transport the beam under the loss criteria
  – The achromat consists of 4 FODO cells, each containing 2 dipoles and 2 quadrupoles. What is the minimum length of the dipole?
  – The beam trajectory has a maximum transverse orbit deviation of 2 cm from the magnet center in the quadrupoles. What is the maximum gradient of the quadrupole that can be used under the loss criteria?
  – Estimate the maximum dipole field when the loss criteria is 10^{-6} per meter instead
  – Estimate the minimum dipole length when the H^- beam is injected at 8 GeV kinetic energy, and the loss criteria is 10^{-5} per meter